IITRI Project D6087
FINAL REPORT

THEORETICAL STUDY OF PRODUCTION OF UNIQUE GLASSES IN SPACE

Prepared for:

National Aeronautics and Space Administration
Marshall Space Flight Center, Ala. 35812

Attention: R. L. Nichols

IITRI

IIT RESEARCH INSTITUTE
Ceramics Research
10 West 35th Street
Chicago, Illinois 60616

THEORETICAL STUDY OF PRODUCTION OF UNIQUE GLASSES IN SPACE

FINAL REPORT
1 July 1973 - 31 January 1975

Contract No. NAS8-29850
IITRI Project No. D6087

May 23, 1975

Prepared by:

D. C. Larsen
J. L. Sievert

Prepared for:

National Aeronautics and Space Administration
George C. Marshall Space Flight Center
Alabama 35812

TABLE OF CONTENTS

TABLE OF CONTENTS (Continued)

LIST OF FIGURES

LIST OF FIGURES (Cont.)

LIST OF TABLES

THEORETICAL STUDY OF PRODUCTION OF UNIQUE GLASSES IN SPACE

1.0 INTRODUCTION AND SUMMARY

This program deals with the glass forming potential of unique systems that cannot be obtained by conventional earth processing. The objective of this program is to determine if the weightless, containerless nature of space processing can be utilized to produce the glassy form of such materials.

Glass formation is approached from the kinetic viewpoint. The overall objective is to develop analytical functional relationships describing nucleation and crystal growth in various supercooled liquids. The time and temperature dependent relationships of nucleation and crystallization (intrinsic properties) are used to relate glass forming tendency to extrinsic parameters such as cooling rate through computer simulation.

A thorough understanding of nucleation and crystallization kinetics provides a priori knowledge of the ability of a given system to form a glass. This will facilitate the development of improved glasses by providing a firm theoretical/analytical basis for improved manufacturing techniques such as in-space manufacture. The ultimate objective of space manufacture is to produce technically significant glasses by extending the Earth-limited regions of glass formation for certain compositions, or by achieving glass formation in other compositions that are not glass formers based on empirical Earth observations.

Single oxide systems were studied initially to aid in developing workable kinetic models and to indicate the primary materials parameters affecting glass formation. The literature was reviewed and critically analyzed, and kinetic equations were developed for homogeneous and heterogeneous nucleation and subsequent crystal growth. For homogeneous nucleation the crystal embryos are created due to local fluctuations in the structure of the liquid phase. If the nucleation is heterogeneous, the phase change process is initiated (enhanced) by the presence of foreign nuclei. The kinetic relationships derived were applied to known

glass formers and non-glass formers. It was found that the models qualitatively predict earth-observed behavior for these systems.

The theory and analytical expressions developed for simple systems was then extended to complex oxide systems. The concept here is to develop sufficient analytical relationships to permit the prediction of the intrinsic glass forming properties of unique systems, with the goal of utilizing the in-space environment in producing technically improved glasses. For complex systems that do not exhibit glass formation on earth, it is believed that the extrinsic effect of heterogeneous nucleation often is the major cause. Unfortunately, the analytical treatment of heterogeneous nucleation phenomena requires much property data that are not readily available. To circumvent this problem the empirical evidence of the phase change process available through North American Rockwell's air suspended laser melting experiments (NAS8-28991) was employed. Coupling the information present in the filmed melting and subsequent crystallization of mullite, the material being studied by Rockwell, with IITRI's developed analytics permitted prediction of the intrinsic glass forming region of this complex material. The analytical treatment involved several first order approximations, but the results indicate that it is technically feasible to produce mullite glasses in the weightless, containerless environment present in an earth-orbiting materials processing laboratory.

2.0 TECHNICAL DISCUSSION

The concept of glass forming tendency derives from the definition of glass. Morey[1] has defined glass an an "inorganic substance in a condition which is continuous with, and analogous to, the liquid state of that substance; but which, as a result of having been cooled from a fused condition, has attained so high a degree of viscosity as to be for all practical purposes rigid." Hence, glass-forming materials are ones in which there is sufficient transient bonding in the melt to produce a highly viscous liquid upon cooling. In the general sense, Morey's restriction of glasses to only inorganic materials can be relaxed to include organic materials as well. The supercooled amorphous state of aggregation of matter comprising a glass is unstable relative to the solid crystalline state. Therefore, glass forming tendency is related to the mechanisms and parameters that prevent the liquid-solid transformation from occurring. Studies of the crystalline transformation can be approached from structural, thermodynamic, and kinetic viewpoints. We have chosen to adopt a kinetic viewpoint since in general glass formation is not related to whether or not a given material can form a glass, but rather how fast must the liquid be cooled from its fused condition to do so.

Therefore, we consider a material to be a glass if it can be cooled from its liquid state rapidly enough to avoid a certain predetermined degree of crystallization. The kinetics of crystallization of a liquid are determined by two parameters, the nucleation rate and the crystal growth rate. The liquid-solid transformation occurs by a two-step process of nucleation of crystalline embryos and subsequent growth. Nucleation and growth rate temperature dependence are illustrated qualitatively in Figure 1. Temperature $T_1 = T_m$ is the thermodynamic fusion temperature where the solid and liquid phases are in co-existence. Above T_m the material is in the liquid phase. As the liquid is supercooled below T_m, growth can theoretically occur between temperatures T_m^- and T_3. However, the embryo nucleation that is

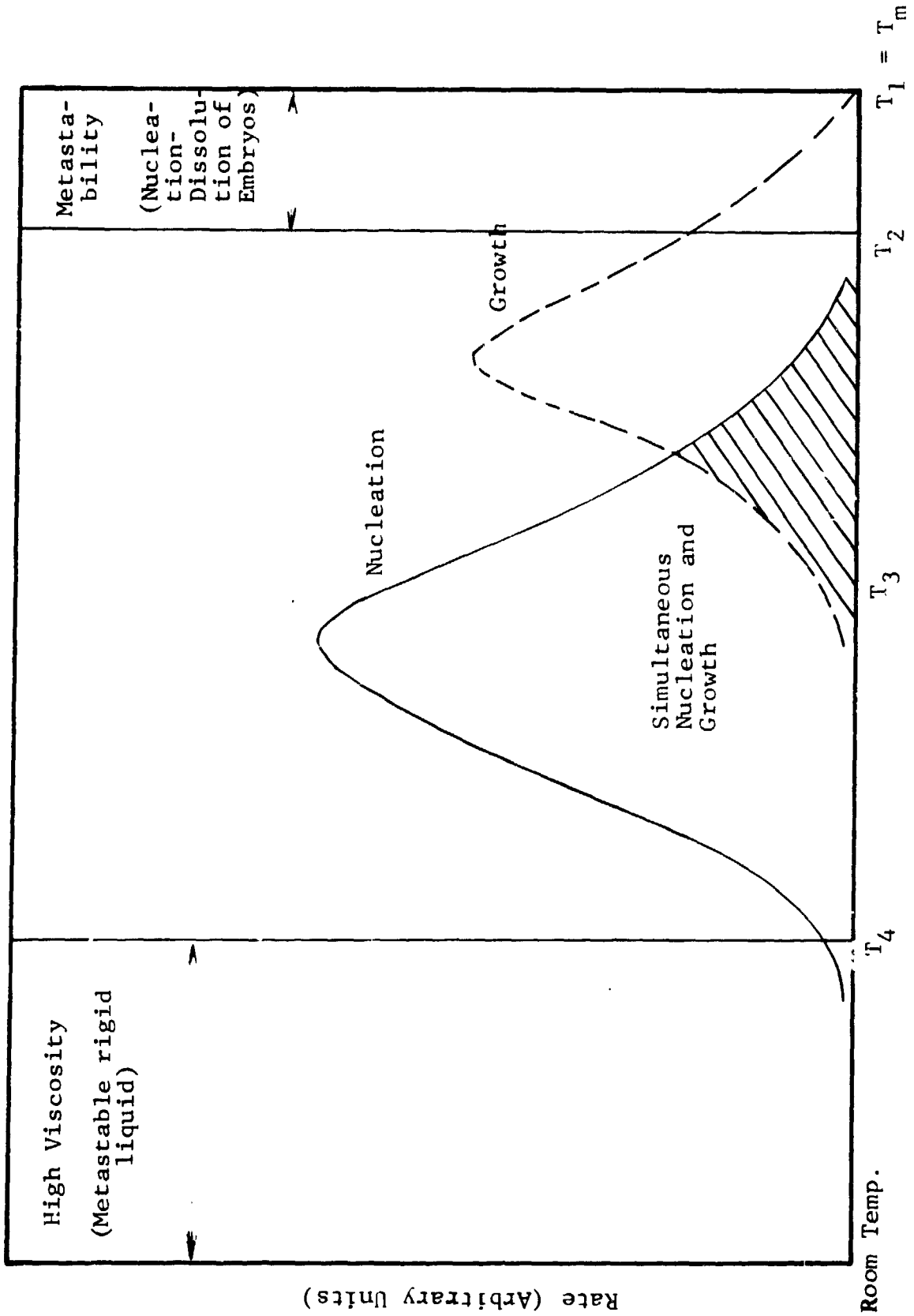

Figure 1 NUCLEATION AND GROWTH RATE OF CRYSTALS IN GLASS AS FUNCTION OF TEMPERATURE

necessary before growth can proceed only occurs between temperatures T_2 and T_4. In the temperature region bounded by T_2 and T_3 nucleation and growth occur simultaneously, i.e., conditions are favorable for the complete crystallization transformation process, nucleation and growth. Therefore, the $(T_2 - T_3)$ temperature region is most critical to the prediction of glass formation.

The present program deals with characterizing the nucleation and growth characteristics of several materials, and presentation in a form similar to Figure 1. With the analytical relationships describing nucleation and crystal growth, computer-simulated melt-quench experiments provide information regarding the cooling rates necessary for glass formation (i.e., cooling rates necessary to pass through the $(T_2 - T_3)$ temperature region rapidly enough to prevent crystallization).

The kinetic treatment of glass formation necessarily starts with derivations of nucleation and growth expressions. In the following sections these parameters are discussed in some detail. Succeeding sections will deal with the volume fraction transformed and critical cooling rates, initial computer-modeled results on single component systems, a discussion of the problems in predicting the behavior of complex multi-component materials, and the use of empirical evidence to permit the analytical treatment of complex non-glass formers.

3.0 KINETICS OF GLASS FORMATION

The information presented in this section results from a critical review of the literature regarding the kinetics of glass formation. We have tied together various author's treatments of the basic science of the phase change process. This provides the basis for our modeling studies on unique systems to follow.

Equations describing the kinetics of homogeneous nucleation, with allowance for transient effects, are developed. The effect of the presence of nucleating heterogeneities is also discussed. Models for subsequent crystal growth are presented. Finally, the method of relating the volume fraction of material transformed to the crystalline state to applied cooling rate through computer simulation is discussed.

3.1 Theory of Homogeneous Steady State Nucleation

A supercooled liquid is a metastable phase relative to the solid phase as indicated by free energy considerations. The liquid system below the fusion temperature T_m tends toward thermodynamic stability by lowering its free energy through the crystalline transformation. The existence of a supercooled liquid phase below T_m (i.e., a glass) is the consequence of 1) a surface energy barrier between the solid and liquid state, and 2) the kinetically inhibited movement of molecules that prevents arrangement in an ordered system (i.e., crystalline phase).

The process initiates as statistical molecular density fluctuations causing clustering of molecules or atoms. The clusters are called nuclei, embryo particles of solid crystalline (transformed) material (transformation to the solid crystalline phase can be considered merely as molecular rearrangement into an ordered structure). In tending toward thermodynamic stability there is a volume free energy decrease as an embryo is created (i.e., in the transformation from liquid to crystalline). However, the formation of an embryo means the formation of a boundary, the embryo-liquid interface, with a resulting system free energy gain due to the interfacial surface energy. Jackson (2) discusses the

stability of such a nucleus in an undercooled liquid with respect to these two phenomena. For small embryos the surface area is large relative to the volume, so that the surface energy dominates embryo behavior. Small embryos can decrease the total free energy of the system (liquid and nuclei) by shrinking to reduce their surface area (i.e., dissolving into the liquid melt). Larger size crystalline embryos are controlled by the volume free energy term. Large nuclei can reduce the total free energy of the system by growing larger, creating more transformed crystalline material (more ordered, more stable). A balance between these tendencies defines the critical size nucleus. A nucleated embryo smaller than the critical size will dissolve. A nucleated embryo larger than the critical size will continue to grow.

Consider a liquid melt at temperature T with order fluctuations. This system can be described as a steady state concentration of ordered regions (crystalline in structure) of various sizes. The change in free energy of the system, ΔF, due to a local fluctuation creating a spherical nucleus may be expressed:

$$\Delta F = -\frac{4}{3}\pi r^3 \Delta f_v + 4\pi r^2 \Delta f_s \qquad (1)$$

where r = embryo radius

Δf_v = free energy difference between the liquid and solid state, per unit volume

Δf_s = interfacial (surface) free energy between the phases, per unit area.

The system free energy change has a maximum value, ΔF^*, for some critical nucleus radius, r^*. The critical nucleus size, r^*, represents the smallest size embryo that can grow with a decrease in free energy to form stable nuclei. The critical nucleus size is derived as follows. Differentiating ΔF with respect to r gives

$$\frac{\partial \Delta F}{\partial r} = -4\pi r^2 \Delta f_v + 8\pi r \Delta f_s \qquad (2)$$

Expression (1) has a maximum, ΔF^*, for a value of $r = r^*$ satisfying

$$\frac{\partial \Delta F}{\partial r} = 0 \qquad (3)$$

Setting the r.h.s. of expression (2) equal to zero and solving for $r = r^*$ we obtain

$$r^* = \frac{2\Delta f_s}{\Delta f_v} \qquad (4)$$

Evaluating the expression for ΔF (Equation (1)) for $r = r^*$ yields ΔF^*, the minimum work required to form a stable nucleus:

$$\Delta F^* = \frac{16\pi}{3} \frac{\Delta f_s^{\,3}}{\Delta f_v^{\,2}} \qquad (5)$$

The term ΔF^* is the thermodynamic barrier to the nucleation process of forming stable nuclei. We now turn our attention to obtaining the surface and volume terms in ΔF^* in more useful form.

Turnbull (3) has shown that the liquid-crystal surface tension, Δf_s, can be related to the heat of fusion, Δh_f, by the expression

$$\Delta f_s = \frac{\Delta h_f}{\alpha} N^{-1/3} V_m^{-2/3} \qquad (6)$$

where Δh_f = molar latent heat of fusion of the crystalline phase (cal mole^{-1})

N = Avagadro's number ($\sim 6 \times 10^{23}$ molecules mole^{-1})

V_m = molar volume of the crystalline phase (cc/mole).

The dimensionless term α relates the proportionality of Δh_f and Δf_s, and is constant for a given type of fluid (3). For metals $\alpha \sim 2$, for more complex materials $\alpha \sim 3.3$. Therefore, α has an approximate range

$$2 \leq \alpha \leq 3.3 \qquad (7)$$

The parameter α is defined such that physically the reciprocal of α, $1/\alpha$, is equal to the number of monolayers per unit area of crystal which would be melted at T_m by an enthalpy $\Delta H = \Delta f_s$.

The volume free energy difference between the liquid and solid states, Δf_v, is expressed:

$$\Delta f_v = \int_{T_m}^{T} \left(\frac{\Delta s_f}{V_m} \right) dT \tag{8}$$

which is estimated for small supercooling $\Delta T = T_m - T$:

$$\Delta f_v = \frac{\Delta s_f \Delta T}{V_m} \tag{9}$$

where Δs_f is the molecular entropy of fusion (cal $mole^{-1} deg^{-1}$). Since the entropy of fusion is related to the heat of fusion, Δh_f (cal/mole)

$$\Delta s_f = \frac{\Delta h_f}{T_m} \tag{10}$$

the expression for Δf_v (per unit volume) can be expressed

$$\Delta f_v = \frac{\Delta h_f}{T_m} \frac{\Delta T}{V_m} \tag{11}$$

At large degrees of undercooling $\Delta T = T_m - T$, this expression is modified by the factor T/T_m

$$\Delta f_v \text{ (large } \Delta T) = \frac{\Delta h_f}{T_m} \frac{\Delta T}{V_m} \frac{T}{T_m} \tag{12}$$

Limiting our analysis to the case of small undercooling, use of Equations (6) and (11) for Δf_s and Δf_v, respectively, permits expression of r* from Equation (4) in more useful terms:

$$r^* = \frac{2 T_m V_m^{1/3}}{\alpha N^{1/3} \Delta T} \tag{13}$$

For clusters (embryo) below T_m with radius $r < r^*$, nuclei form and dissolve because the surface energy involved in cluster formation is greater than the free energy change accompanying solid formation. For $r > r^*$, continuous nuclei growth will occur since the surface energy is growing only proportional to r^2 while the bulk (volume) free energy term involved in solid formation is growing proportional to r^3. Above T_m crystalline embryo are unstable. Critical cluster radii are illustrated in Figure 2 for various oxide systems.

The thermodynamic barrier to nucleation, F^*, is expressed in more useful terms, employing Equation (6) and (11) for Δf_s and Δf_v respectively:

$$\Delta F^* = \frac{16\pi}{3} \frac{\Delta h_f T_m^2}{\alpha^3 N \Delta T^2} \tag{14}$$

It will be convenient to express ΔF^* in terms of another dimensionless parameter, β, defined (9) such that

$$\Delta s_f = Nk\beta = R\beta \tag{15}$$

where k = Boltzmann's constant

R = 1.987 cal mole $^{-1}$deg^{-1} = gas constant.

The heat of fusion, Δh_f, thus becomes

$$\Delta h_f = \Delta s_f T_m = R\beta T_m = Nk\beta T_m \tag{16}$$

The parameter β has range

$$1 \leq \beta \leq 10 \tag{17}$$

with $\beta = 1$ for monatomic liquids. More complex structures have higher entropies of fusion, with β approaching $\beta = 10$.

The expression for ΔF^* (Equation 14) is expressed in terms of β:

$$\Delta F^* = \frac{16\pi}{3} \frac{k\beta T_m^3}{\alpha^3 \Delta T^2} \tag{18}$$

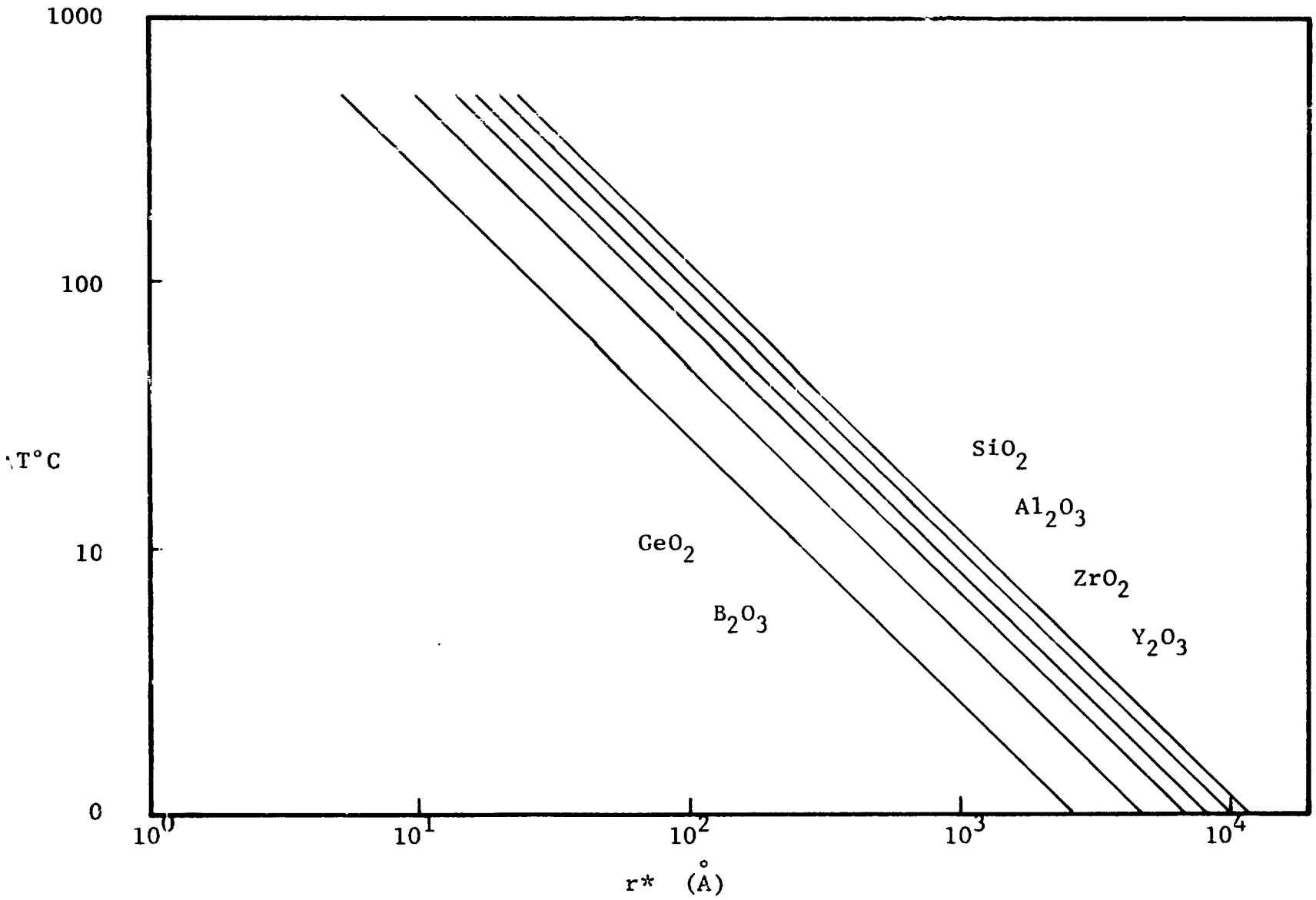

Figure 2 RADII r* OF CRITICAL EMBRYOS AS FUNCTION OF UNDERCOOLING ΔT FOR VARIOUS OXIDES (α = 2)

Having developed an expression based on thermodynamics and free energy considerations for the minimum work required for homogeneous nucleation (i.e., the thermodynamic barrier to nucleation), we must now derive an expression for the rate of homogeneous nucleation. If it is assumed that critical size clusters ($r = r^*$) are formed by statistical molecular fluctuations, the nucleation rate will be proportional to a term involving the probability of such a fluctuation, $\exp(-\Delta F^*/kT)$. The steady state nucleation rate involving a Boltzmann-like distribution of critical size nuclei is expressed:

$$I_o = n\nu_n \exp(-\Delta F^*/kT) \qquad (19)$$

where n = number of molecules per unit volume in the system ($n = \frac{N}{V_m} \sim 10^{22}$) and ν_n is a molecular attempt frequency for nucleation.

This result is derived from thermodynamics and thermostatistics. However, the nucleation process involves molecular movement. Therefore, a kinetic or diffusional barrier also exists for the nucleation process. The steady state nucleation rate, I_o (nuclei $cc^{-1}sec^{-1}$), is expressed in general terms

$$I_o = n\nu_n \exp(-\Delta F^*/kT)\exp(-\Delta G'/kT) \qquad (20)$$

where $\Delta G'$ is the activation energy for molecular motion (during nucleation) across the embryo-matrix interface. Thus the nucleation rate (steady state) is a function of (1) the number of molecular or atomistic units available for nucleation, (2) a frequency factor describing how often the molecules attempt to jump across the liquid-nucleus boundary, (3) a thermodynamic barrier to nucleation, the minimum work required to form a stable nucleus, and (4) a kinetic barrier to nucleation, involving the activation energy for molecular rearrangement.

If the molecular motion involved in nucleation is treated as an activated process (4), a diffusional rate constant for

nucleation, D_n, can be defined such that

$$D_n = a_o^2 \nu_n \exp(-\Delta G'/kT) \tag{21}$$

where a_o is the molecular jump distance.

Combining Equations (20) and (21) yields the following expression for the steady state nucleation rate:

$$I_o = \frac{nD_n}{a_o^2} \exp(-\Delta F^*/kT) \tag{22}$$

The problem now arises as how to evaluate the nucleation diffusional rate constant, D_n. For liquids which crystallize without change in composition (single component systems, for instance) long range diffusion processes are not required. All of the atomic or molecular units required for the ordered crystalline structure are in the local vicinity of the liquid-crystal interface. This type of transformation is termed non-reconstructive. The activation energy, $\Delta G'$, for diffusion at the liquid-crystal interface will be roughly the same order of magnitude as the activation energy for viscous flow. This is the case for a liquid transforming to solid without change in composition since the movements of the atoms or structural units on the nucleation surface is similar to the reorientation of structural units and bond switching in the flow of a viscous liquid. Therefore, in this simple case, the nucleation diffusional rate constant, D_n, will be approximately equal to the self diffusion coefficient of the undercooled liquid:

$$D_n \sim D_s \tag{23}$$

The liquid self diffusion coefficient, D_s, is related to the bulk viscosity, η, through the Stokes-Einstein relation

$$D_s = \frac{kT}{3\pi a_o \eta} \tag{24}$$

where a_o is the diameter of the diffusing species.

Therefore, for the case of a single component substance, or a more complex liquid that crystallizes with no change in composition, the steady state nucleation rate is expressed (for small degrees of undercooling below T_m)

$$I_o = \frac{nkT}{3\pi a_o^3 \eta} \exp\left[\frac{-16\pi\beta T_m^3}{3\alpha^3 T \Delta T^2}\right] \qquad (25)$$

where all terms have been previously defined.

The general temperature dependence of the homogeneous nucleation rate described by Equation (25) is shown in Figure 1. For small degrees of undercooling below T_m, ΔF^*, the thermodynamic barrier, is large since Δf_v, the volume free energy change in the transformation is small. This results in low nucleation rates. With further supercooling Δf_v increases until $\Delta F^* \sim \Delta G'$, the kinetic barrier to nucleation. This condition results in maximum nucleation rate. For a large ΔT the nucleation rate decreases to a negligible level as $\Delta G' > > \Delta F^*$.

In the case where a compositional change accompanies the liquid-solid transformation, the steady state nucleation rate (Equation (25)) must be modified to account for the long range diffusion processes that are required for molecular rearrangement. This subject will be treated in Section 5.0.

3.1.1 Time-Dependent Homogeneous Nucleation

In this discussion transient effects on nucleation are considered. Glass forming tendency is related to how fast the system can pass through the region of simultaneous nucleation and growth (i.e., the $(T_2 - T_3)$ region shown in Figure 1). The time spent at any particular temperature level may then be less than the time required to establish a steady nucleation rate (i.e., the time required to build up the required Boltzmann-like distribution of embryos).

Incorporation of time-dependence into nucleation theory has been treated by Hillig (5) and Hammel (4), and takes the form

$$I_t = I_o e^{-\tau/t} \qquad (26)$$

where I_t = transient nucleation rate
I_o = steady state nucleation rate
t = time.

Hammel (4) has expressed the parameter τ (after Collins(6)) as:

$$\tau = \frac{144kTT_m V_m^{1/3}}{N^{1/3}\alpha a_o^2 \Delta s_f \Delta T^2 D} \qquad (27)$$

where D is the appropriate diffusion coefficient (given by the Stokes-Einstein equation for transformation without change of composition) and all other terms have been previously defined. This equation was derived for the ideal case of instantaneous cooling from T_m to T.

Hillig (5) derived an approximate expression for τ using random walk diffusion theory to describe the mean time $\bar{t}$ to build a critical nucleus:

$$\tau = \bar{t} = \frac{\pi V_L^2 r^{*2}}{4DV_m^2 X^2} \qquad (28)$$

where V_L and V_m are the mole volumes of the liquid and precipitating phase, respectively, D is again the appropriate diffusion coefficient ($D = D_s$ for crystallization without change in composition), and X is the mole fraction of the precipitating phase in the liquid (i.e., X = 1 for crystallization without change in composition).

Hillig's $\bar{t}$ parameter has been shown (4) to more accurately describe time-dependence of the nucleation rate, based on

correlation with experimental results. Therefore, we shall employ Equations (26) and (28) when simulating nucleation in computer generated melt-quench experiments.

The nature of transient effects on nucleation rate is illustrated qualitatively in Figure 3. Due to diffusional effects successively longer times are required to achieve steady state nucleation at successively lower temperatures. If the hypothetical material whose nucleation characteristics are shown in Figure 3 is cooled from T_m to T_1 detectable nucleation would be avoided at any cooling rate*. However, a detectable level of homogeneous nucleation occurs between temperatures T_1 and T_2. In order to avoid this nucleation in a melt-quenching experiment the temperature region T_1 - T_2 must be passed through in less than time t_2. If this glass were successfully quenched to temperature T_6, for instance, it could be held at this temperature level for a period of time t_6 before detectable nucleation would occur (e.g., for annealing).

As shall be discussed in Section 5.0, the transient nucleation formulation provides one possible way of dealing with multicomponent systems where long range diffusion processes are required for molecular rearrangement.

3.2 Heterogeneous Nucleation

Thus far we have only treated the case of homogeneous nucleation in pure substances free of impurities, insoluble particles, etc. Foreign surfaces present in the liquid, such as container walls or insoluble particles, however, tend to reduce the barrier to nucleation represented by the surface energy between the liquid and solid phases. As a result the critical embryo size is reduced and the "supercooling temperature" is raised. The "supercooling temperature" is the temperature T_2 where the first detectable nucleation is observed upon cooling from the melt. This effect is shown qualitatively in Figure 4.

*For many materials $T_1/T_m \sim .8$

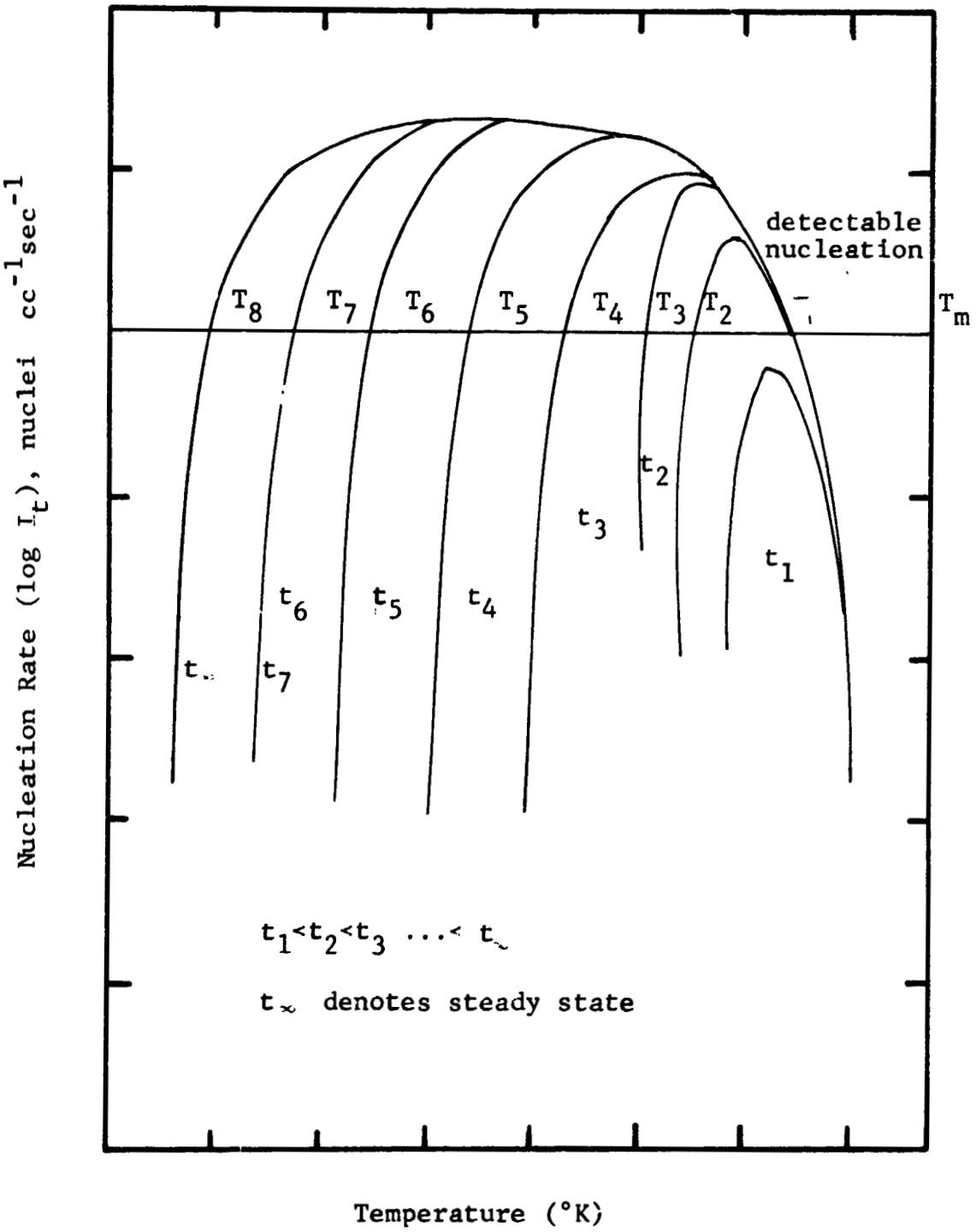

Figure 3 NUCLEATION RATE SHOWING TRANSIENT EFFECT

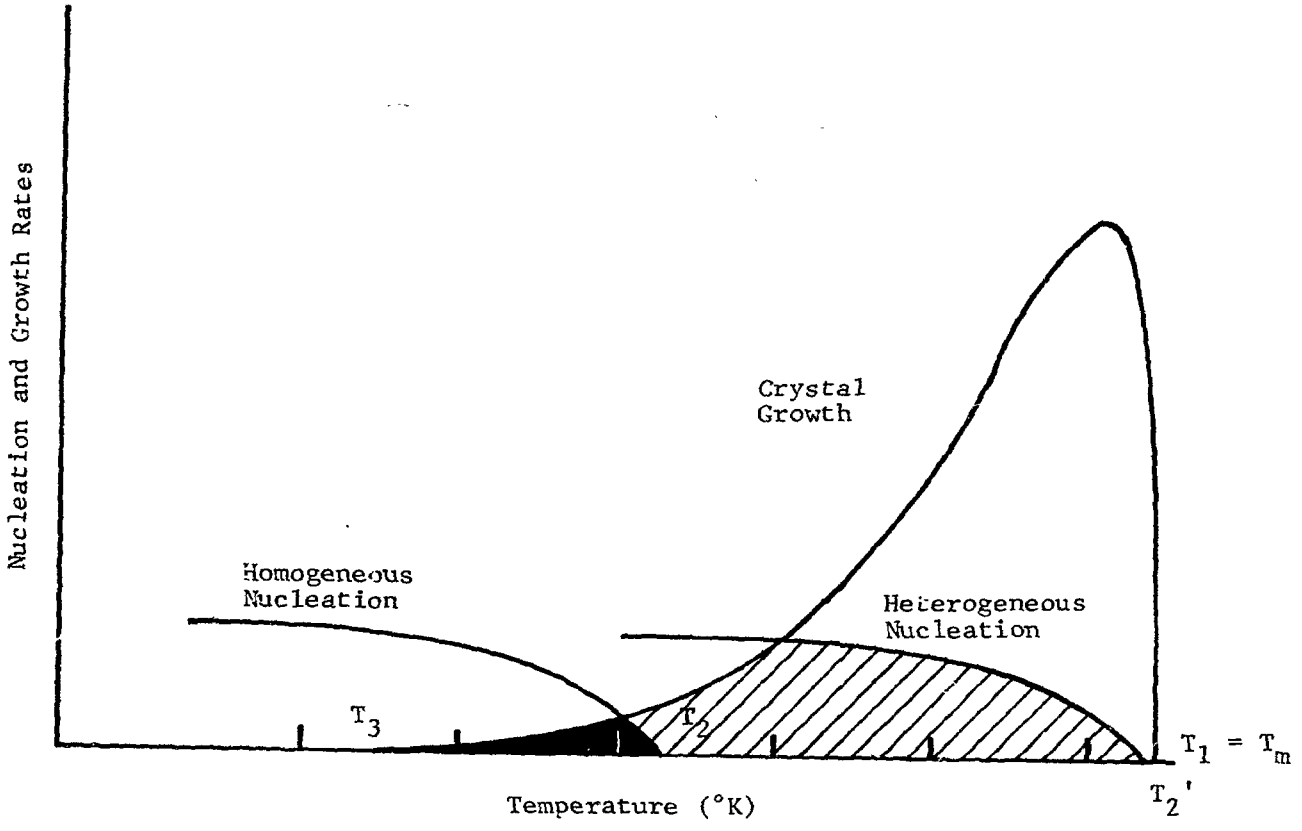

Figure 4 EFFECT OF HETEROGENEOUS NUCLEATION ON GLASS FORMING TENDENCY

At heterogeneous surface sites the computation of the critical embryo size becomes complicated because of the various surface energies involved and the particular geometry of the embryo surface. Furthermore, the wettability of the foreign surface by the liquid must be taken into account.

For our present purposes we shall only treat the effect of heterogeneous nucleation qualitatively, following the treatment of several authors (references 2, 4, 5, 7-9) in order to illustrate the nature of the analytical expressions.

The work term for heterogeneous nucleation, ΔF^*_θ, given generally as

$$\Delta F^*_\theta = f(\theta) \cdot \Delta F^* \tag{29}$$

where the factor $f(\theta)$ is expressed

$$f(\theta) = \frac{(2 + \cos\theta)(1 - \cos\theta)^2}{4} \tag{30}$$

The angle θ is a function of the balance of surface tensions and is given by:

$$\cos\theta = \frac{\sigma_{sL} - \sigma_{s\beta}}{\sigma_{L\beta}} \tag{31}$$

where σ_{sL}, $\sigma_{s\beta}$ and $\sigma_{L\beta}$ are the interfacial energies between the solid-liquid, solid-impurity surface, and the liquid-impurity surface, respectively.

The lowering of the net interfacial energy in heterogeneous nucleation depends on how well the impurity surface wets the nucleating phase in the presence of the liquid.

Therefore, if heterogeneous nucleation sites are present the minimum work required (thermodynamic barrier to nucleation) to form a stable nucleus is reduced. The treatment is further complicated by the fact that the concentration of nuclei deriving from a heterogeneous mechanism will be some function of the concentration of impurity sites present, and not given simply by a nucleation rate formulation.

3.3 Crystal Growth Kinetics

Once formed by homogeneous or heterogeneous nucleation mechanism, stable nuclei will continue to grow at a rate determined primarily by the rate at which the atoms necessary for growth can diffuse to the surface of the crystal, and by the ease with which they can free themselves from the attractions of their neighbors in the liquid phase and form new bonds in the specific positions determined by the structure of the growing crystal (10). The fundamental concept here is that growth is considered in terms of molecular rearrangement.

Crystal growth is either interface-controlled or diffusion-controlled. Interface-controlled growth occurs when the rate controlling step occurs at the liquid-crystal interface. This normally occurs for single component glasses, for instance, where only short range molecular rearrangement at the liquid-crystal interface is necessary. Diffusion-controlled growth occurs when the rate controlling step is the long range diffusion of a given species in the bulk liquid. Thus, diffusion-controlled growth would normally apply in the case where crystallization is accompanied by a large change in composition, such as for complex multicomponent systems.

3.3.1 Interface-Controlled Growth Kinetics

For this work we shall restrict ourselves to the case of crystallization without change in composition as we have done for the case of homogeneous nucleation in the preceding sections. Thus, we will treat in this section only the mechanisms and kinetics of interface-controlled growth.

Two basic mechanisms have been proposed for interface-controlled growth: continuous growth and lateral growth (11). In continuous growth the crystal interface advances by molecular incorporation which can occur with equal probability everywhere (except for certain anisotropic effects). Lateral growth occurs either by a two-dimensional nucleation mechanism or by a screw dislocation spiral growth ramp mechanism depending on the crystal perfection.

In systems which crystallize without change in composition the nature of the liquid-crystal interface strongly influences the kinetics and morphology of crystallization. Different models for interface controlled growth are each based on a different assumption concerning the interface and the nature of the sites on the interface where atoms are added or removed. Again, it is important to think of crystal growth as merely a molecular rearrangement process.

The general form of the growth velocity for all interface-controlled growth processes is:

$$u = f a_o \nu_g \exp(-\Delta G''/RT)\left[1 - \exp(-\Delta G/RT)\right] \quad (32)$$

where f = fraction of preferred growth sites on the interface (i.e., fraction of sites available for growth, $0 < f \leq 1$).

ν_g = frequency factor for molecular transport at the liquid-crystal interface (during growth).

a_o = distance advanced by the interface in a unit kinetic process (~ molecular diameter).

ΔG = free energy change accompanying the liquid-crystal transformation

$\Delta G''$ = free energy of activation or kinetic barrier for the movement of an atom across the liquid-crystal interface during crystallization (i.e., growth).

The kinetic term $\Delta G''$ involved in growth is not necessarily equal to (or even the same order of magnitude) as the kinetic term involved in nucleation, $\Delta G'$ (Equation (20)). Growth may be governed by atomic movements from a great distance away from the liquid-crystal interface. Nucleation (initiation of the transformation) is governed by atomic movement relatively close to the developing nucleus.

Assuming that we can treat the molecular movements involved in crystal growth as simply activated processes, we can define a diffusion coefficient, or rate constant, for the molecular rearrangement

$$D_g = a_o^2 \nu_g \exp(-\Delta G''/RT) \quad (33)$$

in a manner similar to the case of nucleation described in Section 3.1. The general interface-controlled growth expression (Equation (32)) thus becomes:

$$\mu = \frac{fD_g}{a_o}\left[1 - \exp(-\Delta G/RT)\right] \quad (34)$$

Experience on a variety of pure substances which crystallize without change in composition has indicated that the slow, rate controlling step in the interface growth process is the same molecular process that occurs in the bulk liquid above the thermodynamic fusion temperature, T_m(3). Therefore, in this most straightforward of cases, the rate constant for interface-controlled growth, D_g, will have approximately the same value as the liquid self diffusion coefficient, D_s, and thus be approximated by the Stokes-Einstein relation:

$$D_g \cong D_s = \frac{kT}{3\pi a_o \eta} \quad (35)$$

The free energy change accompanying the liquid-crystal transformation, ΔG, is given by

$$\Delta G = \Delta s_f \Delta T \quad (36)$$

The growth velocity for interface-controlled growth without composition change is thus expressed

$$\mu = \frac{fkT}{3\pi a_o^2 \eta}\left[1 - \exp\left(\frac{-\Delta s_f \Delta T}{RT}\right)\right] \quad (37)$$

or in terms of the β parameter ($\Delta s_f = Nk\beta = R\beta$)

$$\mu = \frac{fKT}{3\pi a_o^2 \eta}\left[1 - \exp\left(\frac{-\beta \Delta T}{T}\right)\right] \quad (38)$$

since

$$R = Nk \quad (39)$$

We will now briefly treat the various models that have been proposed for interface-controlled growth. The models and discussion presented have been taken from Uhlmann (12).

3.3.1.1 Normal (Continuous) Growth

In normal or continuous growth atoms can attach to or be removed from any site on the interface. Thus, there are no preferred growth sites in the interface, and f in Equation (37) becomes unity.

$$\mu = \frac{kT}{3\pi a_o^2 \eta}\left[1 - \exp\left(\frac{-\Delta s_f \Delta T}{RT}\right)\right] \qquad (40)$$

For small departures from equilibrium, this model predicts a linear relation between growth rate, μ, and undercooling, ΔT. For this model to correlate with experimental data the liquid-crystal interface must be rough on an atomic scale.

3.3.1.2 Screw Dislocation Growth

In the screw dislocation model growth occurs at step sites provided by screw dislocations intersecting the interface. The fraction of preferred growth sites, f in Equation (37), is expressed

$$f = \frac{a_o \Delta h_f \Delta T}{4\pi\sigma T_m V_m} \sim \frac{\Delta T}{2\pi T_m} \qquad (41)$$

where it has been assumed that only molecular transport within a molecular diameter, a_o, of the dislocation ledge results in attachment. For small undercooling, ΔT, this model predicts a growth rate which varies with ΔT^2. For the screw dislocation model to apply, the interface must be smooth on an atomic scale, and be relatively imperfect in the crystallographic sense.

3.3.1.3 Surface Nucleation Growth

According to this model growth takes place at step sites provided by two-dimensional nuclei formed on the interface. The

growth rate can be expressed

$$\mu = A\nu\exp(-B/T\Delta T) \tag{42}$$

where the exponential constant is

$$B = \frac{\pi a_o V_m T_m \sigma_E^2}{k\Delta h_f} \tag{43}$$

The term σ_E is the specific edge surface energy of the nucleus. The frequency factor, ν, can be derived from the growth rate constant:

$$\nu = \frac{D_g}{a_o^2} \tag{44}$$

The growth velocity predicted by this model should vary exponentially with the undercooling, ΔT, and for small ΔT should be unobservably low. For this model to correspond to experimental observation the interface must be smooth on an atomic scale and be defect-free.

This comment and the foregoing discussions regarding expected morphology for each of interface-controlled growth models will have application in the experimental stages of our NASA program (to be discussed later). For materials which have not been extensively studied, morphological studies (SEM, etc.) will indicate, by inference, which growth model applies to a given material. Utilizing empirical results of melt-quench experiments to correlate with our kinetic relationships will help to indicate how space processing can be utilized to produce glasses unobtainable on Earth.

3.3.2 Significance of Entropy of Fusion

As discussed by Uhlmann (12) growth rates depend critically on the molecular structure of the liquid-crystal interface. The interface structure, in turn, depends significantly on a bulk thermodynamic property, the molecular entropy of fusion, Δs_f.

For materials characterized by low entropies of fusion ($\Delta s_f < 2R$) the liquid-crystal interface should be rough on an atomic scale, defects should not affect growth, and normal growth kinetics are predicted (i.e., Equation (40)). On the scale of light microscopy the crystal-liquid interface should be non-faceted.

For materials characterized by large entropies of fusion ($\Delta s_f > 4R$) faceted interface morphologies should be observed, defects should be important to growth, and the kinetics of the normal growth model should not apply. Except as limiting cases, the observed growth velocities for large Δs_f materials should not agree well with behavior predicted by screw dislocation model or the surface nucleation model either.

3.4 Volume Fraction Transformed and Critical Cooling Rates

Glass forming tendency can quantitatively be described in terms of the volume fraction of crystalline material formed during a certain quenching operation. Uhlmann (13) has expressed the volume fraction, v_f, crystallized in time, t, (for small v_f) as

$$v_f \sim 1/3\pi I \mu^3 t^4 \qquad (45)$$

where I = nucleation rate (nuclei $cc^{-1} sec^{-1}$)
μ = growth velocity (cm sec^{-1})
t = time (sec).

This relation is valid for interface-controlled growth, and thus applies to single component or congruently melting (i.e., without change in composition) compounds.

The critical cooling rate for glass formation, i.e., the minimum cooling rate necessary to avoid a certain volume fraction of transformed material, can be estimated by a procedure employed by Uhlmann (13). T-T-T (time-temperature-transformation) curves are constructed as illustrated qualitatively in Figure 5. Using Equation (45), the time required to transform a given amount of material is calculated as a function of temperature. A volume

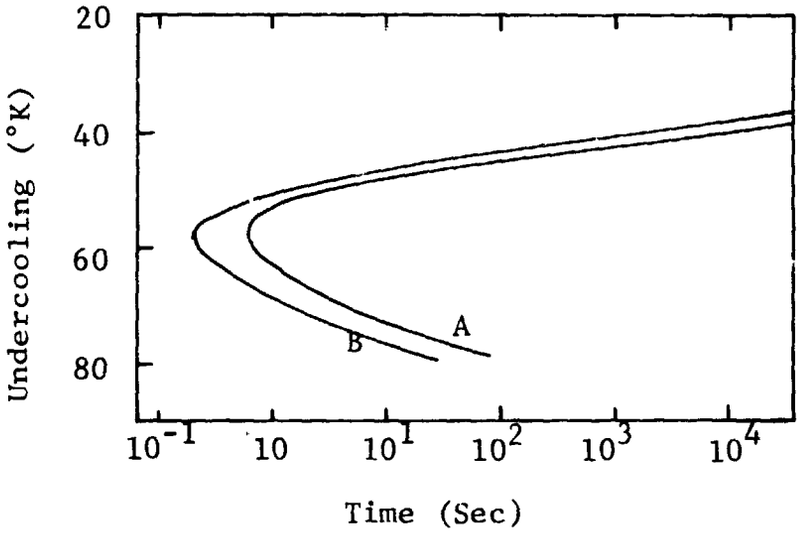

Figure 5 TIME-TEMPERATURE-TRANSFORMATION CURVE (TAKEN FROM UHLMANN (13))

fraction transformed $v_f = 10^{-6}$ is regarded as just-detectable. The data are presented graphically as ΔT vs t in the T-T-T plot. The critical cooling rage can be approximated (13) by the expression

$$\left.\frac{dT}{dt}\right|_{critical} = \frac{\Delta T_N}{\tau_N} \qquad (46)$$

where $\Delta T_N = T_m - T_N$

T_N = temperature at the nose of the T-T-T curve

τ_N = time at the nose of the T-T-T curve.

4.0 COMPUTER MODELED RESULTS FOR SELECTED SINGLE COMPONENT SYSTEMS

The kinetics developed for nucleation and growth are now applied to several materials systems. The well-characterized silica, SiO_2, system is investigated for the purpose of determining the relative importance of the various kinetic and thermodynamic parameters in controlling transformation behavior. The B_2O_3 system is studied to determine if the derived kinetic relationships will predict its good glass forming qualities, and imply a physical reason for the observed behavior. The alumina, Al_2O_3, system is studied to determine if the kinetics can predict the poor glass forming tendency that is observed on earth, and imply a physical reason for this phenomenon.

4.1 The Silica System (SiO_2)

The pertinent materials properties for the silica system to be used in the derived kinetic nucleation and growth expressions are tabulated in Table I. Viscosity data for the silica system are shown in Figure 6, compared with viscosity data for other oxide systems.

The materials parameters were inserted into the derived nucleation and growth kinetics (Equations (25), (26), (28), and (37)), with results illustrated in Figures 7 and 8. The low temperature cut-off in the nucleation rate has been discussed previously. Figure 7 indicates the relative time scale of this effect. A nucleation rate of 1 nuclei $cc^{-1}sec^{-1}$ has arbitrarily (but by popular custom (5)) been taken as the level of detectable nucleation. As illustrated in Figure 7, detectable homogeneous nucleation for SiO_2 does not occur upon cooling from the melt (T_m) until roughly 1700° to 1750°K. Above about 1200°K the thermodynamic barrier to nucleation controls behavior. Below ~ 1200°K the kinetic (diffusional) factor dominates. The peak growth rate for SiO_2 (Figure 8) is roughly 40 Å/min, and occurs at roughly 50°K undercooling below T_m. The crystal growth rate is seen to be zero at T_m, the thermodynamic fusion temperature.

TABLE I

MATERIALS PARAMETERS FOR SiO_2

Δh_f = 2000 cal $mole^{-1}$

T_m = 2000°K

$\Delta s_f = \frac{\Delta h_f}{T_m} = 1$ cal $mole^{-1}K^{-1}$

$\beta = \frac{\Delta s_f}{R} \sim .5$

a_o = 2.5 Å (~ 0-0 distance in SiO_4 tetrahedron)

f = 1 (normal growth assumed)

X = 1 (pure substance)

$V_m = V_L$ = 27.6 cc $mole^{-1}$

η (viscosity): see Figure 6

α = 2.5 (representative value)

N = 6×10^{23} molecules $mole^{-1}$

$n = \frac{N}{V_m} = 2 \times 10^{22}$ molecules cc^{-1}

$\Delta T = T_m - T$

k = Boltzmann's constant = 1.38×10^{-16} erg C^{-1} = 3.3×10^{-24} cal C^{-1}

R = gas constant = 1.987 cal $mole^{-1}deg^{-1}$

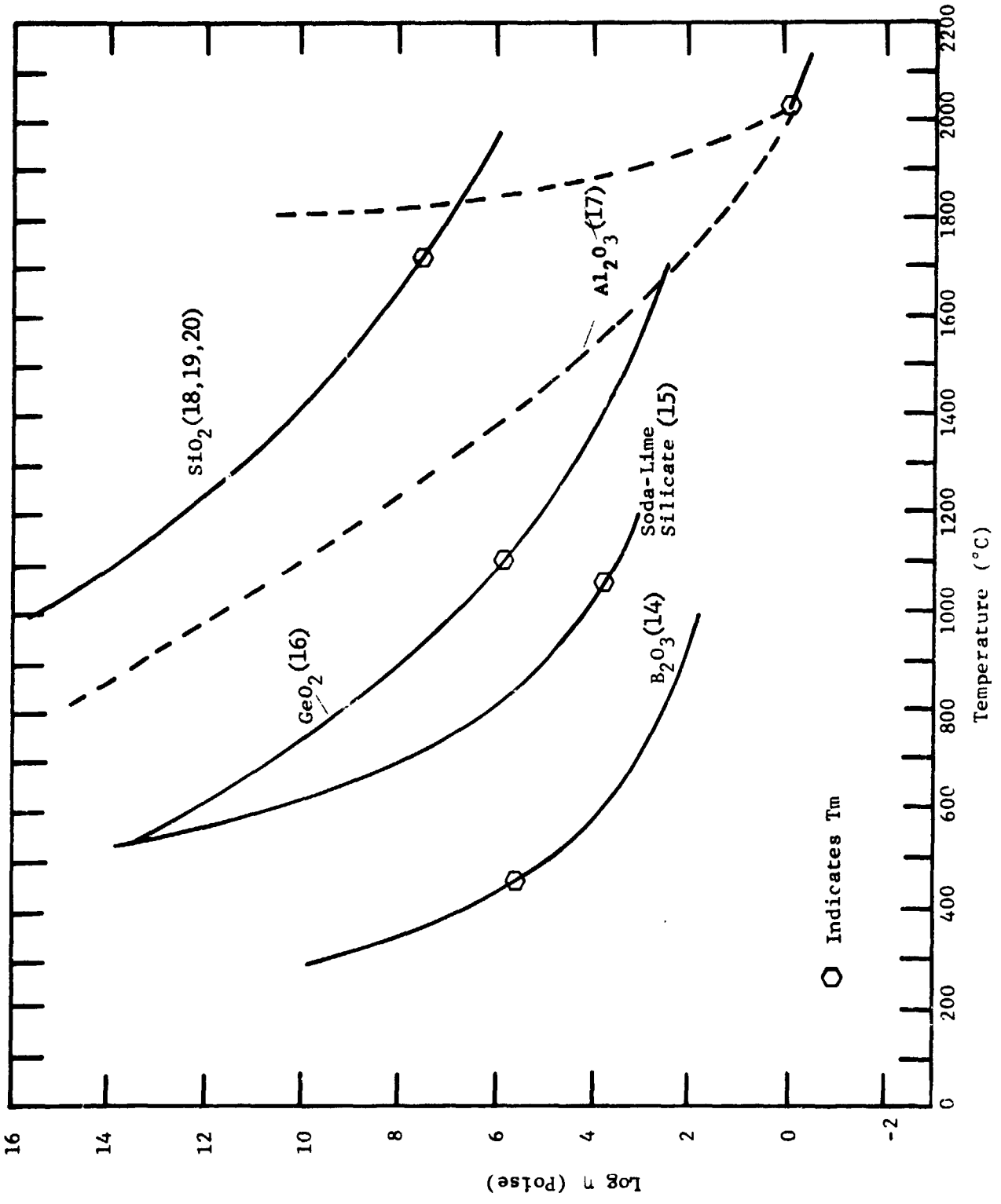

Figure 6. VISCOSITY FOR VARIOUS MATERIALS

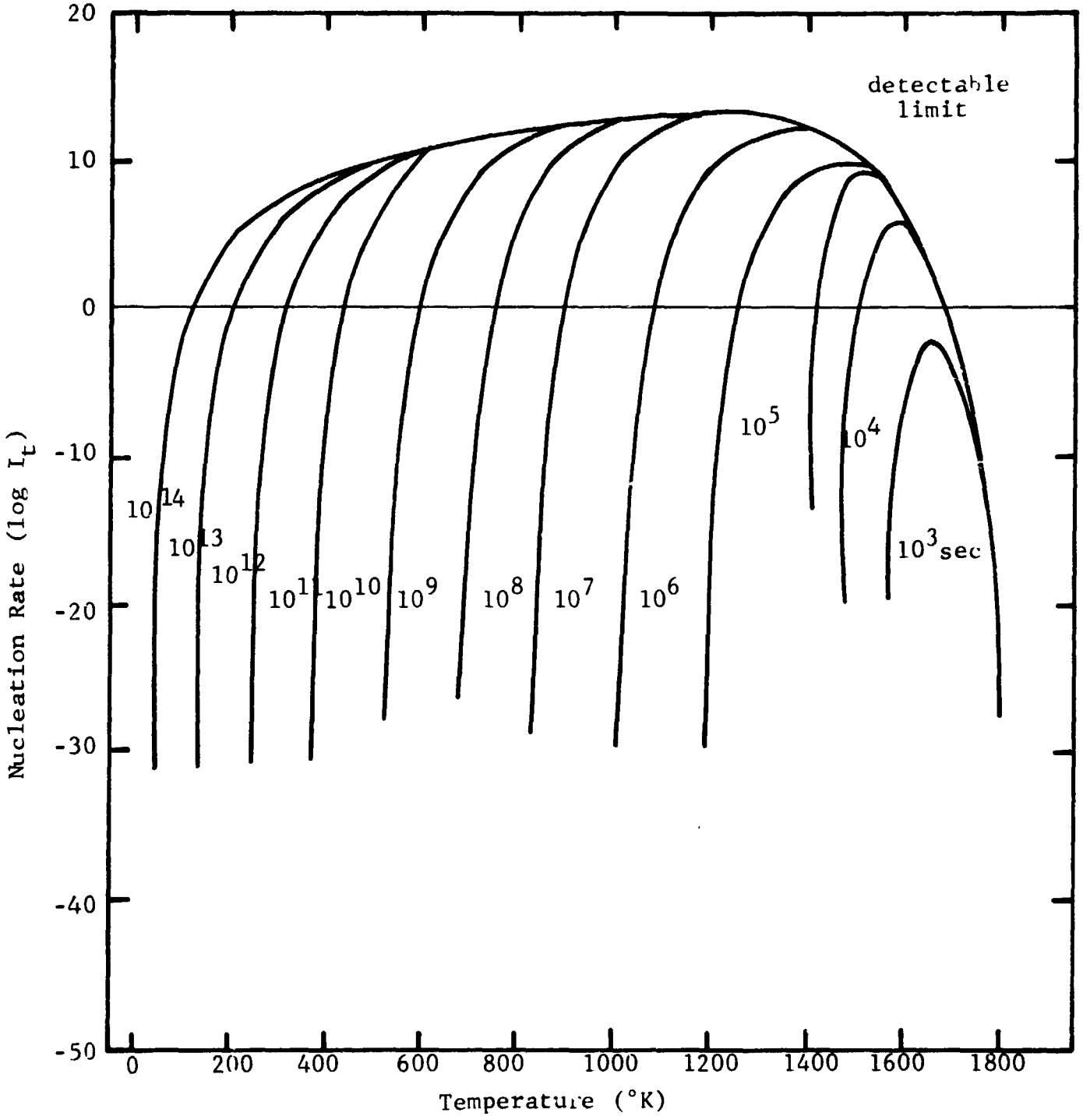

Figure 7 NUCLEATION RATE SHOWING TRANSIENT EFFECT FOR SILICA

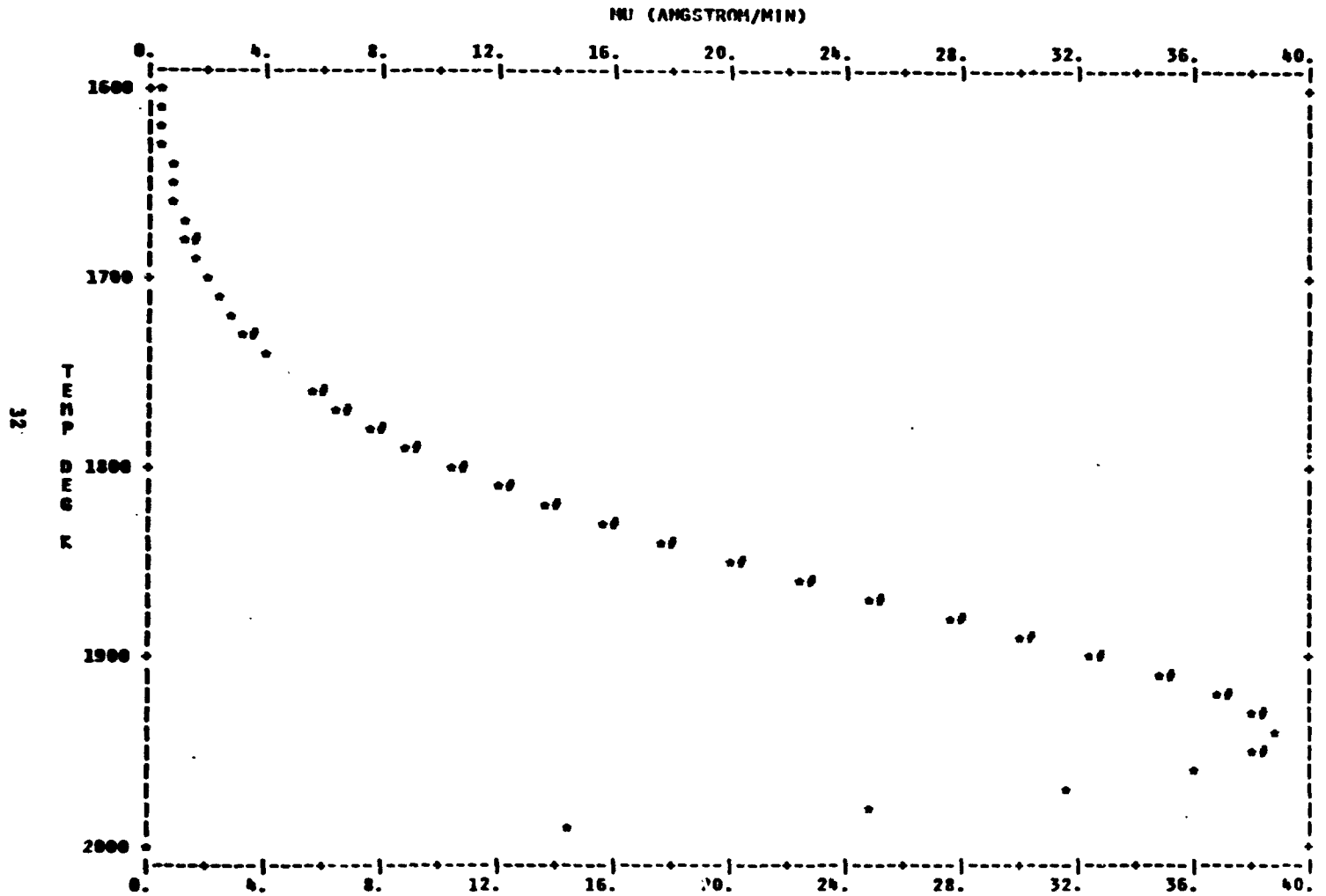

Figure 8 CRYSTAL GROWTH RATE (SiO_2)

For small values of supercooling (temperatures during quench below T_m), the free energy term is dominant and increases with increasing supercooling (i.e., the growth rate increases with decreasing temperature). At large degrees of supercooling below T_m, the kinetic factor (diffusion) begins to control, and the growth rate begins to decrease with decreasing temperature. At temperatures far below T_m the diffusion kinetics dominate: the extremely high viscosity inhibits crystal growth, and the growth rate drops to zero.

The critical temperature region for glass forming tendency, the region of simultaneous nucleation and growth, is illustrated qualitatively in Figure 9 in a "T_2 - T_3" region plot. If homogeneous nucleation only is considered, it is observed that SiO_2 glass formation depends on the ability to pass through the temperature range ~ 1600 - 1700°K rapidly. The transient behavior shown in Figure 7 indicates that this critical region must be tranversed in a time less than approximately 5×10^3 sec to avoid the liquid-crystal phase transformation. This time scale limit is readily attained by commercial earth processing methods.

4.2 Hypothetical Glass-Parametric Study

The computer software that has been developed to generate nucleation and growth behavior using the kinetic and thermodynamic relationships derived in Section 3.0, provides a convenient means of determining which material parameters are of primary importance in determining glass forming tendency. This information is critical to our overall task of investigating the glass forming tendency of unique systems, or in synthesizing systems for space manufacture.

For this purpose a hypothetical glass was postulated that possessed the viscosity-temperature behavior of SiO_2, and the parameters α and β were varied over realistic ranges (i.e., $2 \leq \alpha \leq 3$, $1 \leq \beta \leq 10$). The resulting parametric graphical representations are presented in Figures 10 and 11, and serve to indicate the importance of these parameters on the (steady state)

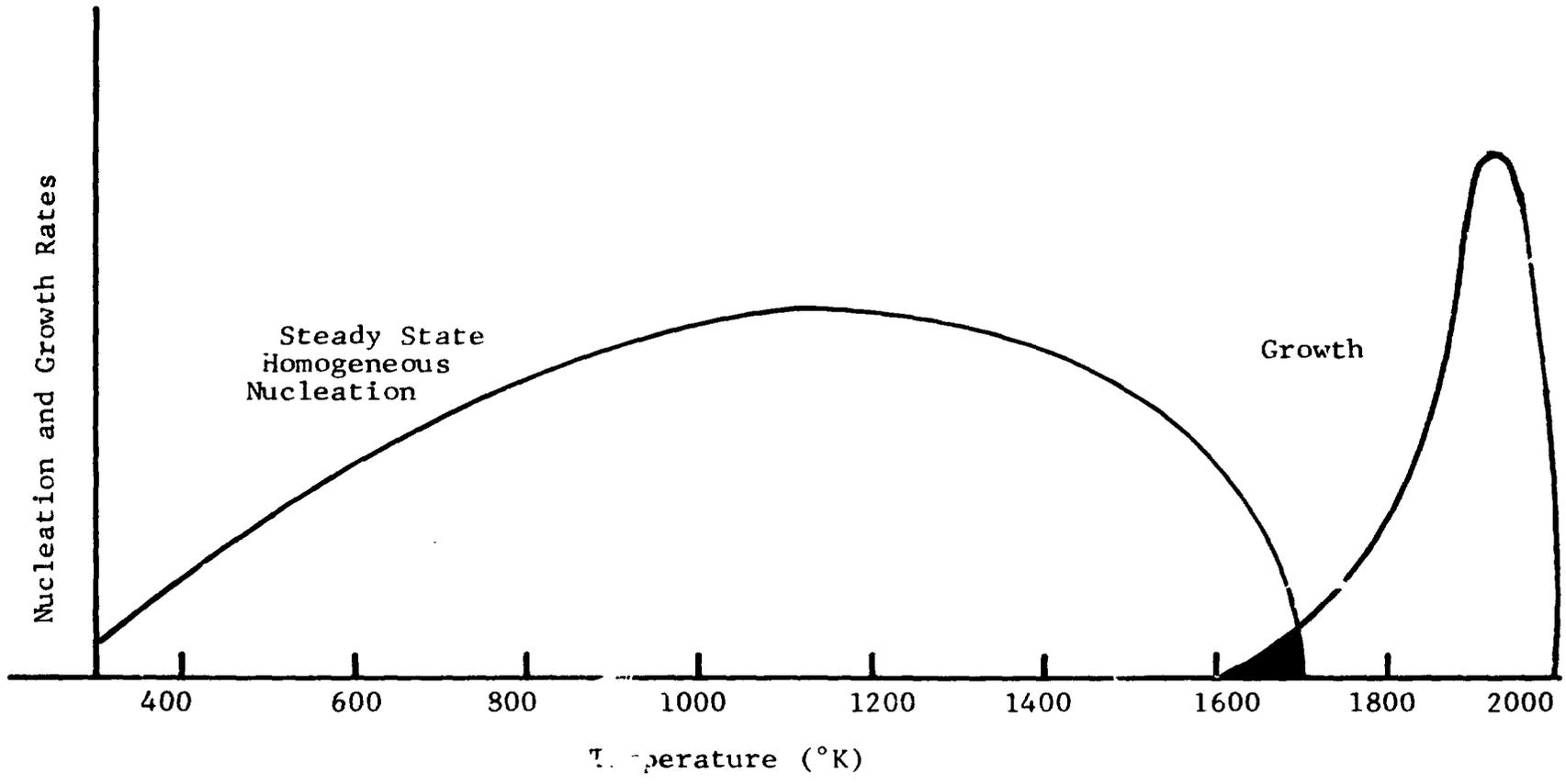

Figure 9 T_2-T_3 REGION NUCLEATION AND GROWTH PLOT FOR SILICA

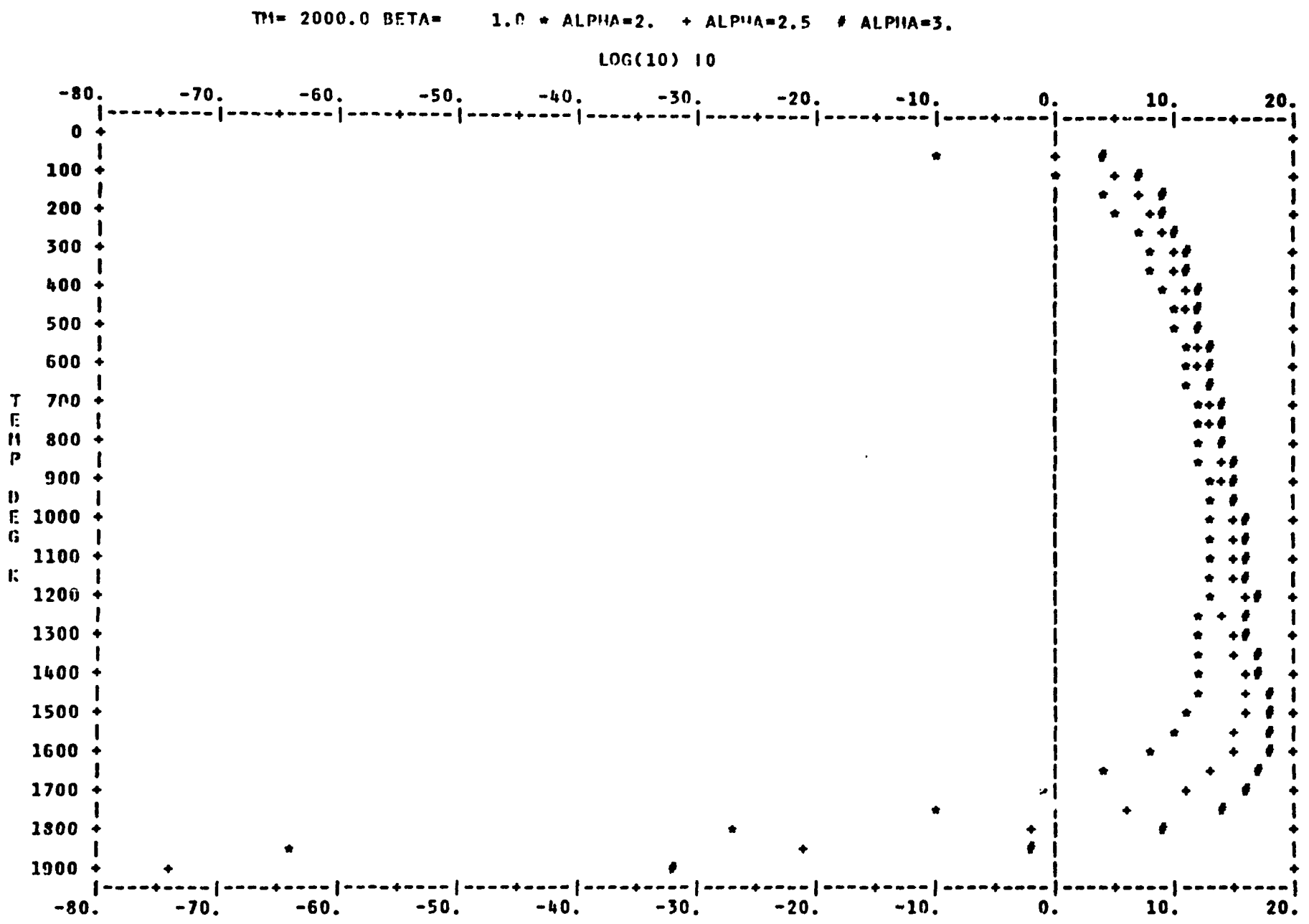

Figure 10 STEADY STATE NUCLEATION RATE FOR A HYPOTHETICAL GLASS (T_m = 2000°K, β = 1, α = VARIABLE); THERMODYNAMIC AND KINETIC BARRIERS

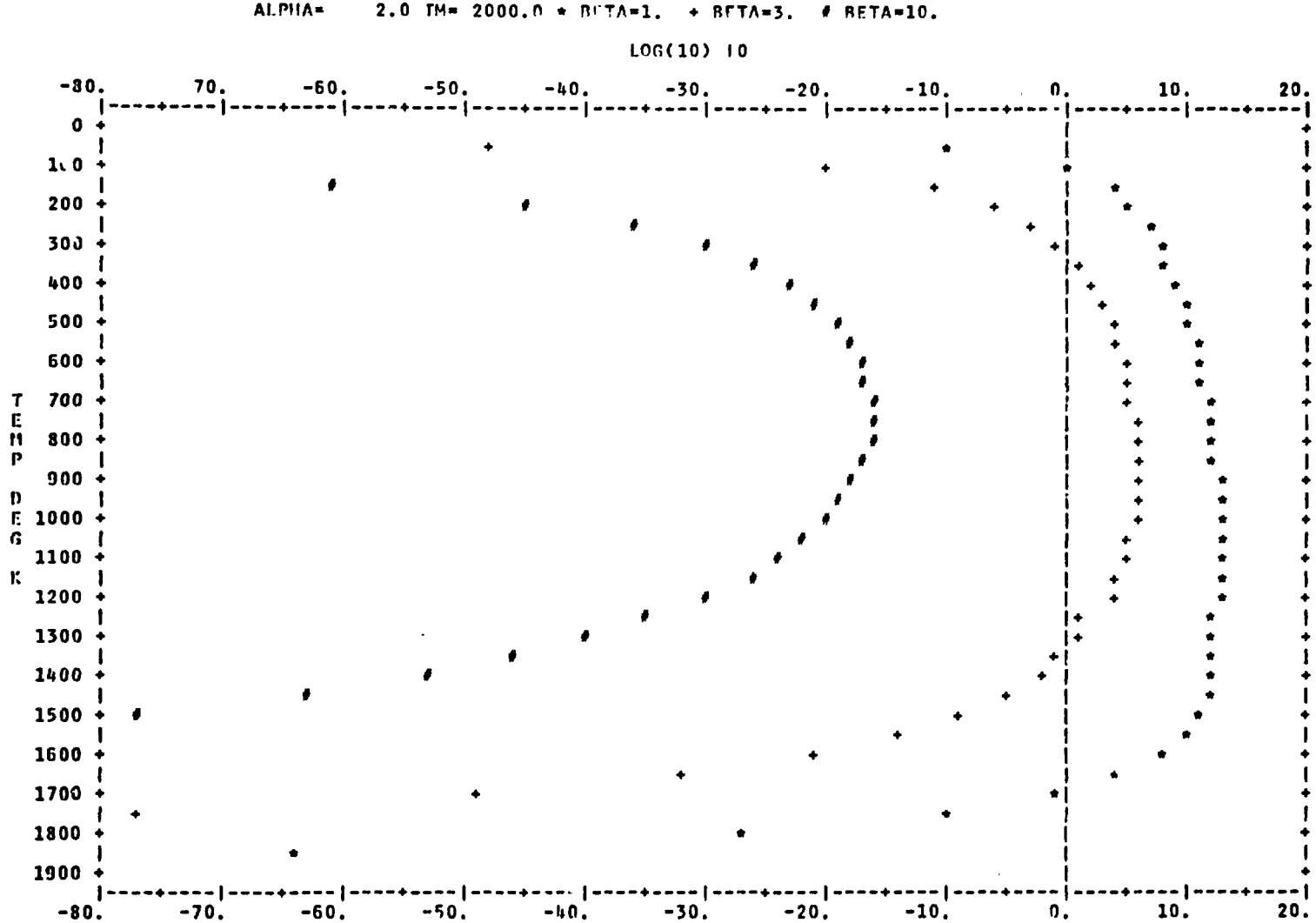

Figure 11 STEADY STATE NUCLEATION RATE FOR A HYPOTHETICAL GLASS (T_m = 2000°K, α = 2, β = VARIABLE); THERMODYNAMIC AND KINETIC BARRIERS

nucleation rate. The horizontal line is the level of detectability of nucleation (assumed to be 1 nucleus per cm^3 per sec). The temperature at which the nucleation curves intersect the horizontal level of detectability line is temperature T_2 shown in Figure 1. Above T_2 no nucleation should be observable. Since nucleation and growth occur simultaneously between T_2 and T_3, we are interested in decreasing $(T_2 - T_3)$; therefore, decreasing T_2 will enhance glass forming tendencies. Additionally, we are interested in material parameters that tend to decrease the slope of the nucleation rate-temperature relationship in the region just below temperature T_2 (this is important due to limitations in cooling rates attainable).

Figure 10 illustrates the effect of α for the hypothetical glass with the β parameter fixed at unity. It is observed that decreasing α decreases T_2, and thus tends to increase glass forming tendency.

Figure 11 illustrates the effect of β for the hypothetical glass, with the α parameter fixed at a value of $\alpha = 2$. It is observed that the β parameter has a larger effect on the nucleation rate than does the α parameter. Temperature T_2 decreases with increasing β.

It is apparent that for enhancing glass forming tendencies large β and small α parameters are required. This is based on the observed decrease in the temperature T_2 and decrease in the slope of the nucleation curve near T_2. This can also be seen by considering the expression for ΔF^*, the free energy of a critical embryo, which represents the magnitude of the barrier to nucleation. A large β represents a material with a large heat of fusion; a complicated structure with a large amount of energy involved in the phase change. A small α represents a material with a large heat of fusion relative to the solid-liquid interfacial free energy. Values for β (or Δs_f) for several systems are shown in Table II.

TABLE II

PERTINENT PROPERTIES OF VARIOUS MATERIALS

Material	Δs_f (cal/mole ^oK)	Δh_f (cal/mole)	β	T_m (^oK)
SiO_2	1	2000	.5	2000
B_2O_3	8.2	5900	4.1	723
GeO_2				
α-Al_2O_3	11.3	26000	5.6	2300
Lithium Silicates	5			
Potassium Silicates	12			
$CaO \cdot Al_2O_3 \cdot 2\ SiO_2$	16.1			
Soda-Lime Glass	8			
Metals	2.3			

Thus far we have only discussed thermodynamic parameters α and β. Since there also exists a kinetic barrier to nucleation and growth, it would be expected that viscosity, η, would be a parameter of primary importance. Uhlmann (13) has discussed the importance of two kinetic parameters on the tendency of a material to be a glass former; (1) a high viscosity at the fusion temperature, T_m, and (2) a rapidly rising viscosity with decreasing temperature below T_m (i.e., large $d\eta/dT$). The latter is related to the position of T_m relative to the glass transition temperature, T_g. We will not elaborate on the parameters η and $d\eta/dT$ in a parametric study. However, they will be considered in subsequent discussions of the glass forming tendencies of B_2O_3 and Al_2O_3.

4.3 The B_2O_3 System

In this section nucleation and growth kinetics are applied to the B_2O_3 system to predict the observed good glass forming quality for this material, and to imply a physical reason for this phenomena. Qualitative indications of glass forming tendency can be obtained by considering only steady state nucleation, ignoring for the moment transient effects. Steady state data represent an upper bound for nucleation behavior.

The pertinent material properties for the B_2O_3 system are tabulated in Table III. The viscosity of B_2O_3 is illustrated in Figure 12. Over the temperature range 250-500°C the literature data shown were averaged and fit to a 6th degree polynomial expression:

$$\log \eta = AT^6 + BT^5 + CT^4 + DT^3 + ET^2 + FT + G \tag{47}$$

with resulting coefficients:

$A = 2.24 \times 10^{-14}$

$B = -4.56 \times 10^{-11}$

$C = 3.82 \times 10^{-8}$

$D = -1.73 \times 10^{-5}$

TABLE III

MATERIALS PARAMETERS FOR B_2O_3

Δh_f = 5900 cal $mole^{-1}$ (reference 21)

T_m = 450°C = 723°K

$\Delta s_f = \frac{\Delta h_f}{T_m}$ = 8.2 cal $mole^{-1}K^{-1}$

$\beta = \frac{\Delta s_f}{R}$ = 4.1

a_o = 2.5 Å (assumed)

f = 1 (assumed normal growth)

X = 1 (pure substance)

α: variable, $2 \leq \alpha \leq 3$

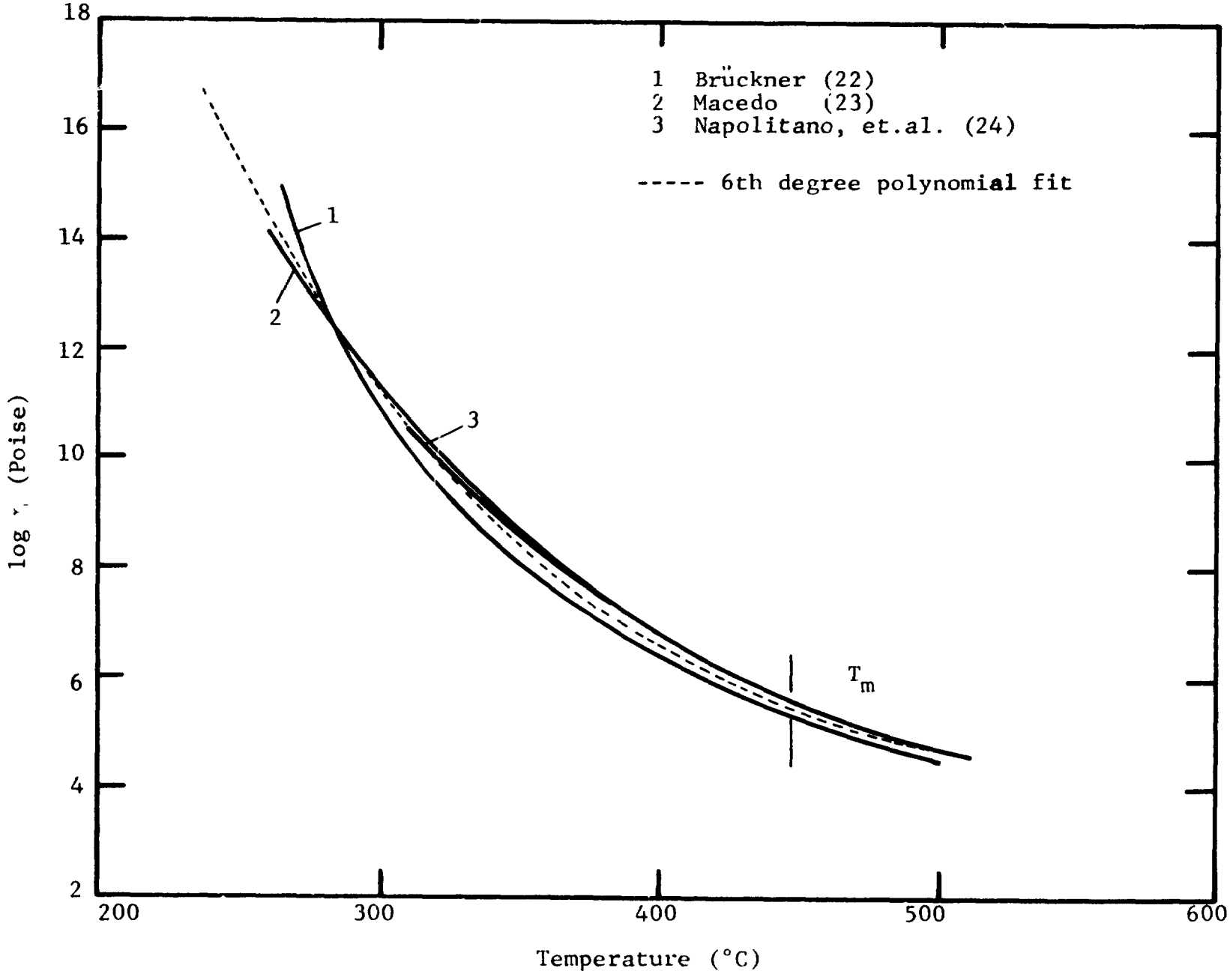

Figure 12 VISCOSITY OF B_2O_3

$$E = 4.81 \times 10^{-3}$$

$$F = -8.9 \times 10^{-1}$$

$$G = 9.77 \times 10^{1}$$

The computer-generated viscosity data for B_2O_3 are also shown in Figure 12 for comparison.

These material properties were inserted into our computer software and the steady state nucleation rate for B_2O_3 computed and plotted for variable α as illustrated in Figure 13. The computed growth rate for B_2O_3 is illustrated in Figure 14. Glass forming tendency for B_2O_3 is deduced from considerations of the nucleation and growth behavior shown in these two figures.

Referring to the growth curve (Figure 14), it is observed that the growth rate for B_2O_3 is zero at T_m, peaks at roughly 700°K, and decays to zero by roughly 625°K. The steady state nucleation rate for B_2O_3 (Figure 13) was computed for the known β parameter ($\beta = 4.1$) and for a probable range of the α parameter. It is observed that for all values of α, the nucleation rate is always below the detectable limit (assumed 1 nucleus per cc per sec), and thus effectively zero. Therefore, although B_2O_3 exhibits a theoretical growth rate much higher than SiO_2 (see Figure 8), critical size crystal embryo are never homogeneously nucleated. These analytical results predict, therefore, that B_2O_3 would be an excellent glass former since it can not be made to nucleate and crystallize when cooling from the melt, regardless of the cooling rate. This prediction is supported by empirical evidence indicating that crystallization of B_2O_3 from a dry melt has never been observed (12).

The parameters of primary importance in describing glass forming tendency from a kinetic standpoint are 1) the magnitude of the viscosity at T_m, 2) the slope of the viscosity-temperature function below T_m, $d\eta/dT$, and 3) the magnitude of the molecular entropy of fusion Δs_f (related to ΔH_f and β). The former two are related to the diffusional barrier and the latter to the thermodynamic barrier to the phase change process, liquid state to

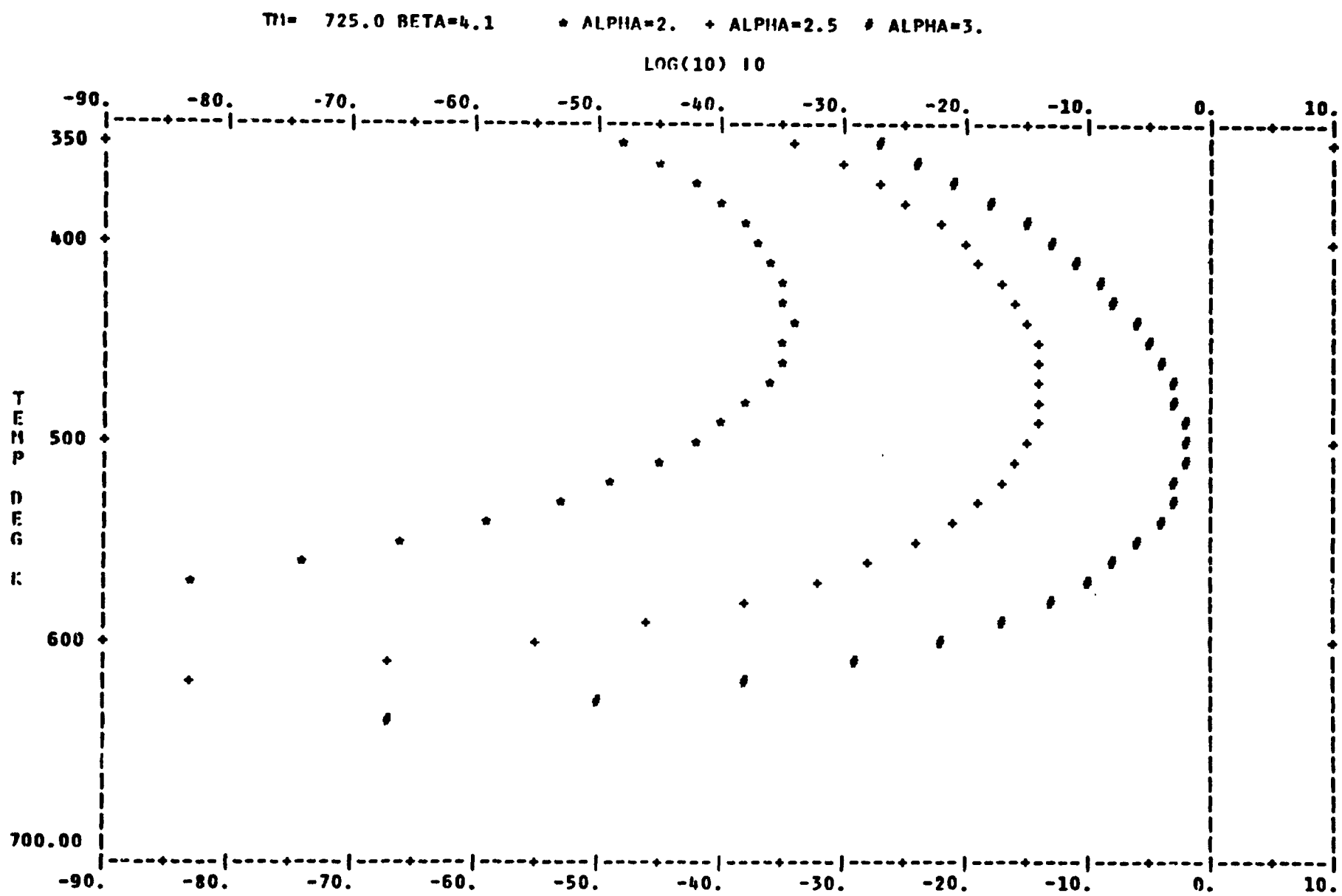

Figure 13 STEADY STATE NUCLEATION RATE FOR B_2O_3 FOR VARIOUS VALUES OF THE α PARAMETER

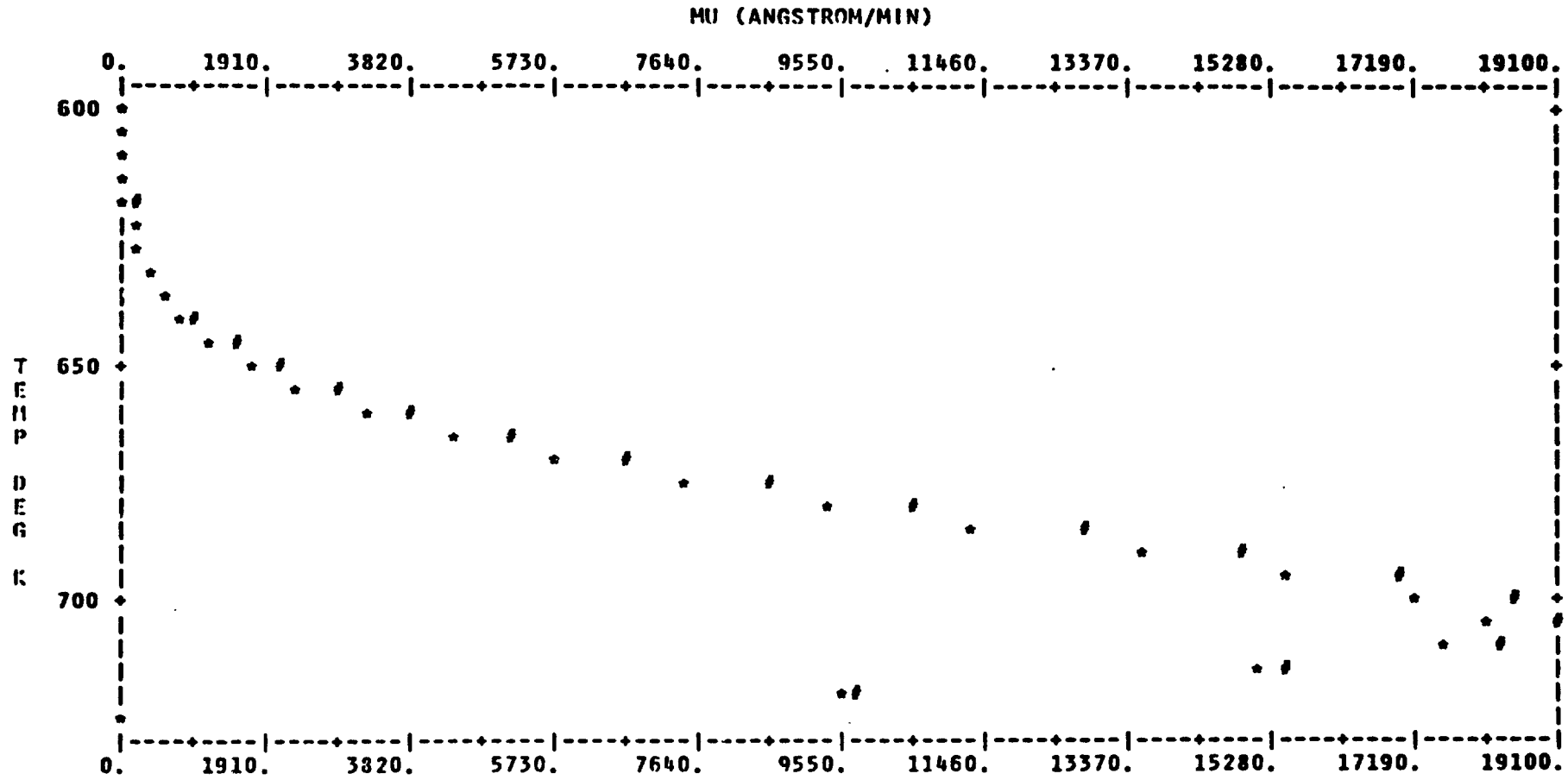

Figure 14 CRYSTAL GROWTH RATE FOR B_2O_3

crystalline state. The magnitude of the melting point viscosity for B_2O_3 is two orders of magnitude less than that of SiO_2 (see Figure 6). This would indicate that nucleation-crystallization should occur more readily for B_2O_3 (lower diffusional, kinetic barrier). Since this is not the case, the factors inhibiting the phase change in B_2O_3 are the higher molecular entropy of fusion (8.2 for B_2O_3, roughly 1.0 for SiO_2), and the steepness of the viscosity-temperature relation below T_m for B_2O_3 ($d\eta/dT$ greater for B_2O_3 than for SiO_2 as shown in Figure 6).

To illustrate the relative importance of Δs_f and $d\eta/dT$ in inhibiting nucleation and crystallization in the B_2O_3 system, we have used our computer system to describe the nucleation behavior of a hypothetical liquid with the viscosity-temperature relation of B_2O_3, but with the molecular entropy of SiO_2 (i.e., $\Delta s_f = 1$). Our hypothetical glass then exhibits the kinetics of a material that will not nucleate and crystallize (B_2O_3) and the thermodynamics of a material that will nucleate and crystallize (SiO_2). The nucleation behavior of this hypothetical material is shown in Figure 15, with the behavior of B_2O_3 ($\Delta s_f = 8.2$) also shown for reference. It is observed that the nucleation rate of the hypothetical liquid is now above the detectable limit. Thus by lowering the thermodynamic barrier to the phase change for B_2O_3 (i.e., Δs_f or β) we are able to produce a hypothetical glass that will nucleate. The growth rate for this hypothetical liquid was computed and is shown in Figure 16. Comparing the relative positions of the nucleation and growth curves for this hypothetical liquid (Figures 15 and 16) indicates its glass forming qualities. For convenience these nucleation and growth curves are qualitatively sketched in a "T_2 - T_3 region" plot in Figure 17. It is observed that a small region of simultaneous nucleation and growth exists between 625 and 650°K. Thus, crystallized B_2O_3 could be obtained upon cooling from the melt (by holding the liquid between 625 and 650°K) if the molecular entropy of fusion (or heat of fusion) could be reduced substantially. This hypothetical example is presented as an indication of how we

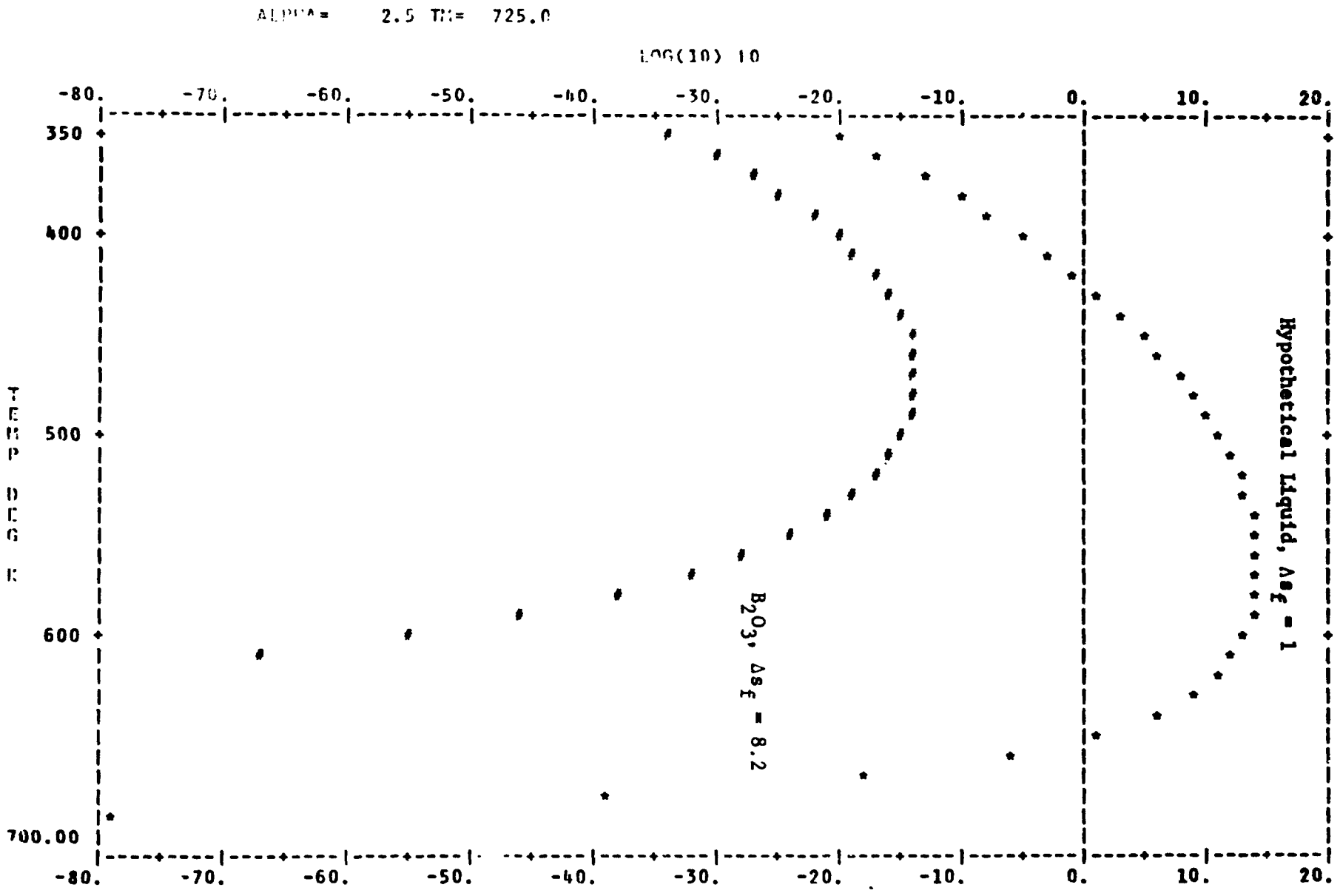

Figure 15 STEADY STATE NUCLEATION RATE FOR B_2O_3 AND A HYPOTHETICAL LIQUID ($\Delta s_{f\ SiO_2}$ = 1, $\eta_{B_2O_3}$)

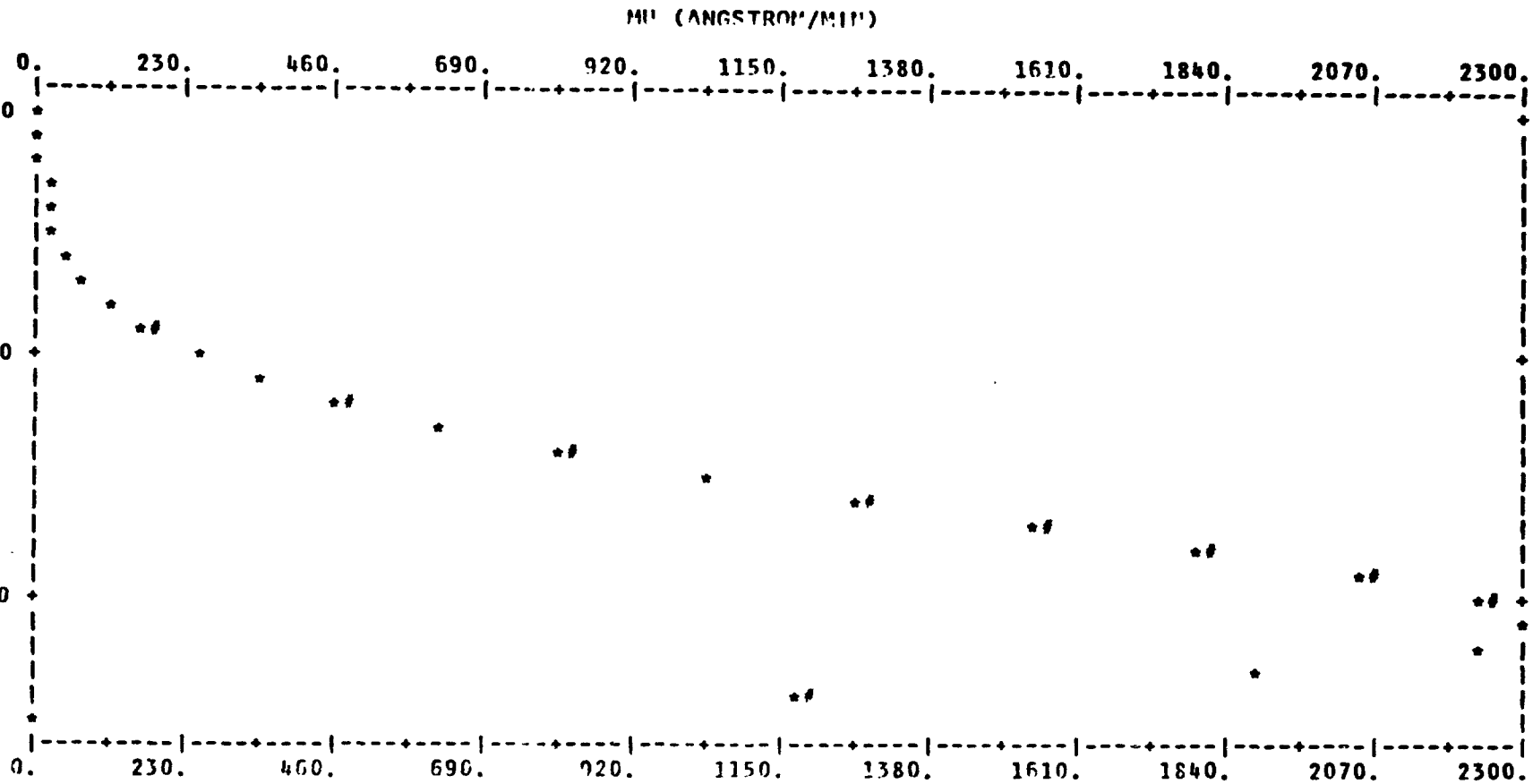

Figure 16 CRYSTAL GROWTH RATE FOR A HYPOTHETICAL LIQUID ($\Delta s_{f\ SiO_2} = 1$, $\eta_{B_2O_3}$)

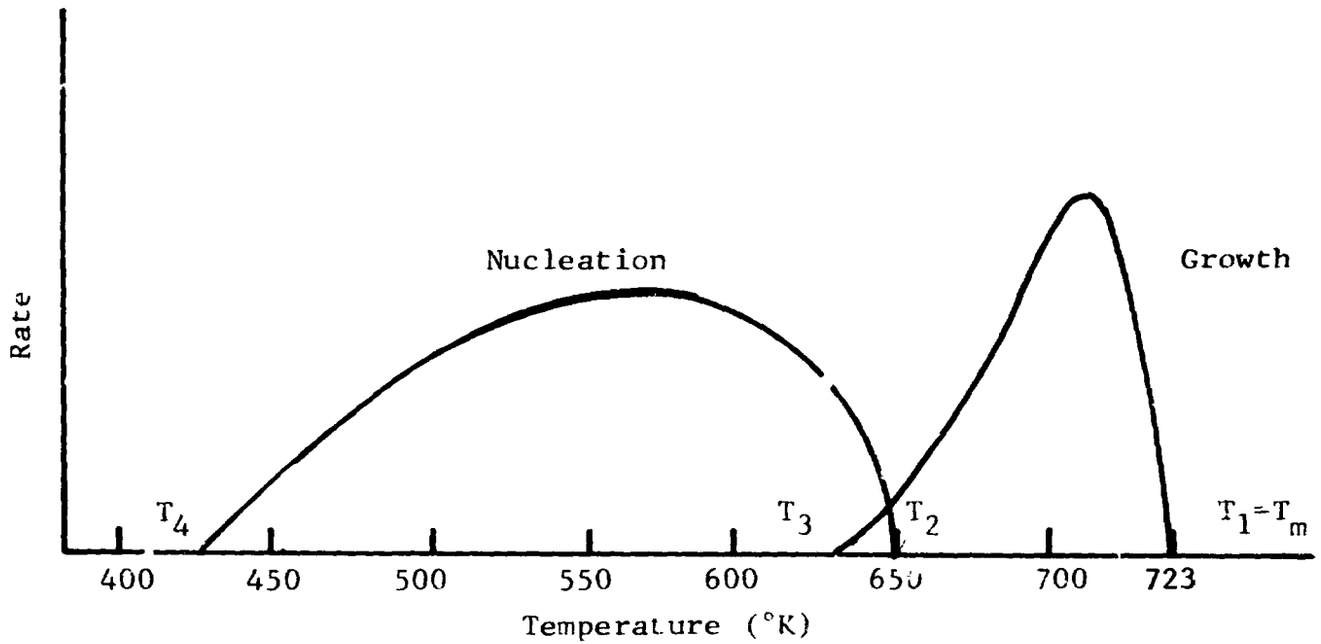

Figure 17 NUCLEATION AND GROWTH CHARACTERISTICS OF A HYPOTHETICAL LIQUID ($\eta_{B_2O_3}$, β_{SiO_2}, $\alpha = 2.5$)

might eventually be able to synthesize materials to exhibit desired nucleation-crystallization tendencies.

4.4 The Al_2O_3 System

Nucleation and growth kinetics also have been applied to the Al_2O_3 system. This system exhibits very poor (non-existent) glass forming tendencies by conventional earth methods. The aim here is to predict this poor glass forming tendency of Al_2O_3 and imply a physical reason for this phenomenon.

The pertinent materials properties for the alumina system are tabulated in Table IV. The major difficulty in describing nucleation and growth kinetics for the Al_2O_3 system is the complete lack of viscosity data below the fusion temperature, T_m. This situation exists since Al_2O_3 has never been observed on earth as a glass (i.e., at temperatures below T_m). Above the melting point, however, data have been reported (17), and are illustrated in Figure 6. With no reference point such as the glass transition, T_g, available, the problem remains as to the shape of the viscosity-temperature curve for Al_2O_3 below T_m. For our purposes we have chosen two cases: 1) extrapolating below T_m with the shape of the B_2O_3 curve (i.e., steep $d\eta/dT$) and 2) extrapolating below T_m with the shape of the SiO_2 curve. These two cases thus represent the upper and lower bounds for $d\eta/dT$ of the various oxides shown in Figure 6. For both cases the extrapolated curves were expressed algebraically using curve fitting techniques for use in our computer software.

The homogeneous nucleation and growth characteristics of Al_2O_3 are summarized in the "T_2 - T_3 region" plot shown in Figure 18. Behavior depicted by solid lines represents the case where Al_2O_3 is assumed to have a $d\eta/dT$ behavior below T_m similar to that of SiO_2 (see Figure 6). The dotted lines in Figure 18 represent the case where the viscosity-temperature dependence of B_2O_3 is assumed below the Al_2O_3 fusion temperature, T_m. Since Al_2O_3 has such a low viscosity at its fusion temperature (melting

TABLE IV

MATERIALS PARAMETERS FOR Al_2O_3

T_m = 2300°K

a_o = 2.5 Å (assumed)

f = 1 (assumed)

Δh_f = 26,000 cal $mole^{-1}$ (reference 21)

$\Delta s_f = \frac{\Delta h_f}{T_m}$ = 11.3 cal $mole^{-1}K^{-1}$

$\beta = \frac{\Delta s_f}{R}$ = 5.65

α = 2, 2.5, 3 (variable)

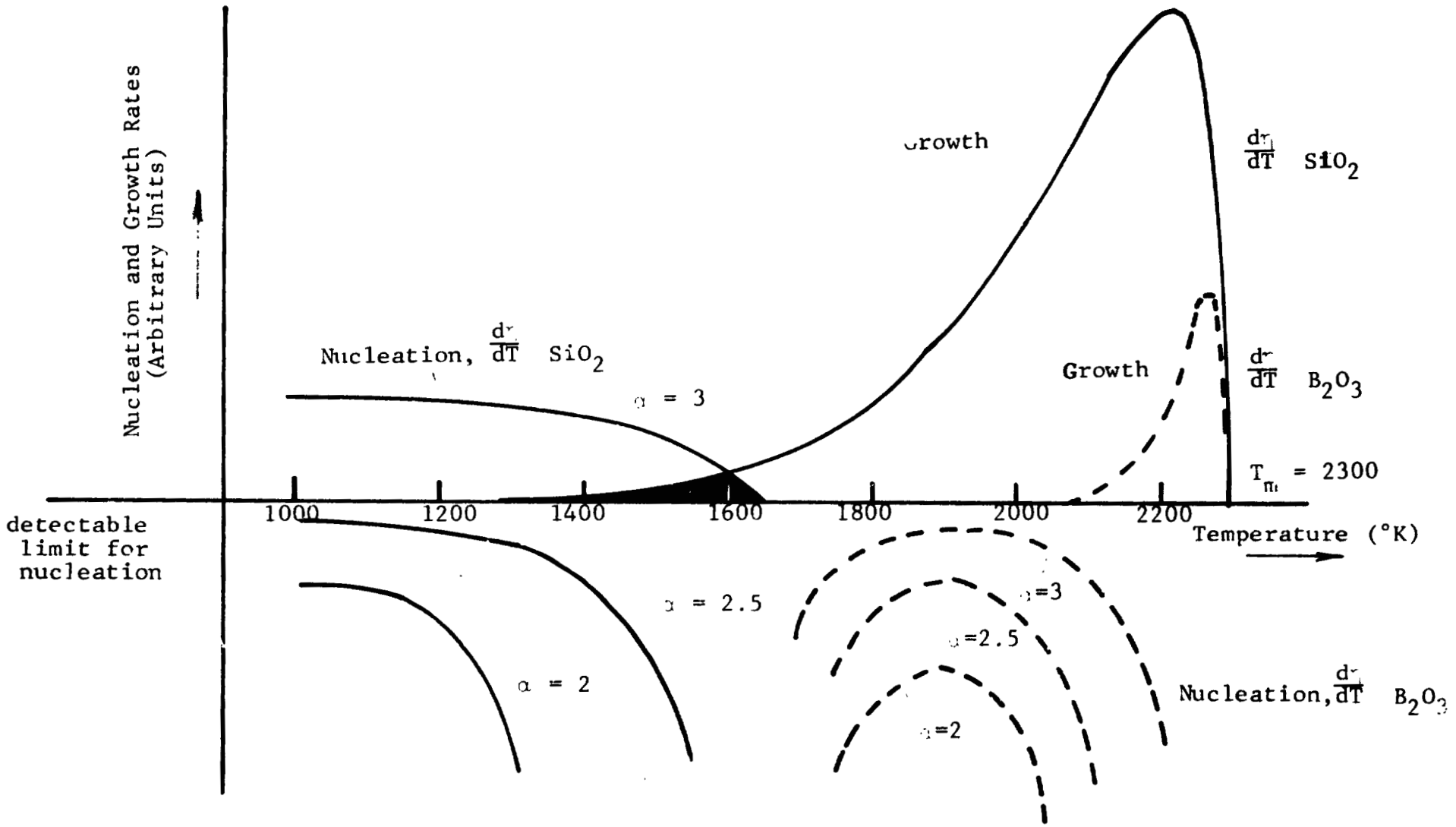

Figure 18 HOMOGENEOUS NUCLEATION AND GROWTH CHARACTERISTICS OF Al_2O_3

point), theoretical growth rates are much higher than for either pure SiO_2 or B_2O_3. Both of the Al_2O_3 growth rate curves shown in Figure 18 have peak magnitudes of $\sim 10^{10}$ Å/min, compared to 40 Å/min for SiO_2 (Figure 8) and 2×10^4 Å/min for B_2O_3 (Figure 14). To illustrate the very large theoretical growth rate of Al_2O_3, the peak growth of B_2O_3 (2×10^4 Å/min) is reached by the alumina system within $\sim 10^{-5}$ °K undercooling below T_m. The 40 Å/min peak growth rate of SiO_2 is reached by Al_2O_3 within $\sim 10^{-8}$ °K undercooling below T_m.

At large degrees of undercooling below T_m, in the diffusion-controlled portion of the growth curve, the steepness of the viscosity-temperature relation is seen to determine the temperature at which the growth rate drops to zero. Since we are dealing with the approximate upper and lower boundaries of the possible viscosity relation of alumina below T_m, this temperature (T_3 in a conventional "T_2 - T_3 region" nucleation and growth plot) lies between approximately 1300° and 2050°K.

The steady state homogeneous nucleation rate for Al_2O_3 is also shown in Figure 18 (for α variable). For the condition where the Al_2O_3 viscosity has the general temperature dependence of B_2O_3 below T_m (steep $d\eta/dT$) it is observed that homogeneous nucleation is below the detectable limit. Where Al_2O_3 is assumed to behave more like SiO_2, which is more probable, it is observed that a detectable level of homogeneous nucleation occurs for $\alpha = 3$. The shaded region shown in Figure 18 thus represents the region of simultaneous (homogeneous) nucleation and crystal growth for Al_2O_3 system.

If homogeneous nucleation and subsequent growth are considered, we have shown that to avoid crystallization upon cooling from the melt the temperature region 1300° to 1625°K must be passed through rapidly. In practice, however, Al_2O_3 is known to crystallize almost immediately upon cooling below the fusion temperature, T_m (2300°K). The reason for this discrepancy is that our analytical predictions of glass forming tendency have not accounted for heterogeneous nucleation. In the case of heterogeneous nucleation, any insoluble impurity or external surface

will serve to lower the size of a critical embryo and thus effectively increase temperature T_2 (the temperature where detectable nucleation first appears upon cooling from the melt). This effect is shown in Figure 19. Temperature T_2, corresponding to homogeneous nucleation, is shifted to a higher temperature (T_2') if heterogeneous nucleation is possible (i.e., if extrinsic nucleation sites are present). As illustrated in Figure 19, simultaneous heterogeneous nucleation and growth can (qualitatively) occur at temperatures just below the fusion temperature, T_m. Most investigators of crystallization phenomena indicate that nucleation appears to initiate heterogeneously in most materials. Thus an extrinsic property controls the glass forming tendency of Al_2O_3, at least on earth where the complete elimination of heterogeneous nucleation sites is not possible. Complete elimination of external nucleation sites in Al_2O_3 is necessary if Al_2O_3 glass is to be obtained since the growth rates are so high. Therefore, Al_2O_3 might be a good candidate for space manufacture since processing could be performed containerless, with no external surfaces acting as nucleation sites. Before the space-processing candidacy of Al_2O_3 is determined, however, several areas must be investigated in more detail. These include: 1) glass quality regarding crystal size and concentration if homogeneous nucleation only is possible (i.e., considering the high growth rates and attainable quench rates from 1625° to 1300°K, perhaps enough crystalline phase would be nucleated homogeneously to yield a poor quality glass even with space processing), and 2) insoluble impurity levels attainable in Al_2O_3 precursor materials (i.e., perhaps enough impurity sites will be available for heterogeneous nucleation to make elimination of surface nucleation sites (crucible wall) through space processing only a second order improvement).

Clearly, if space processing is to be employed to eliminate heterogeneous nucleation sites leading to high quality glasses, then the mechanisms of heterogeneous nucleation must be well known before candidate materials can be chosen with any confidence. This presents a very formidable problem since a purely analytical

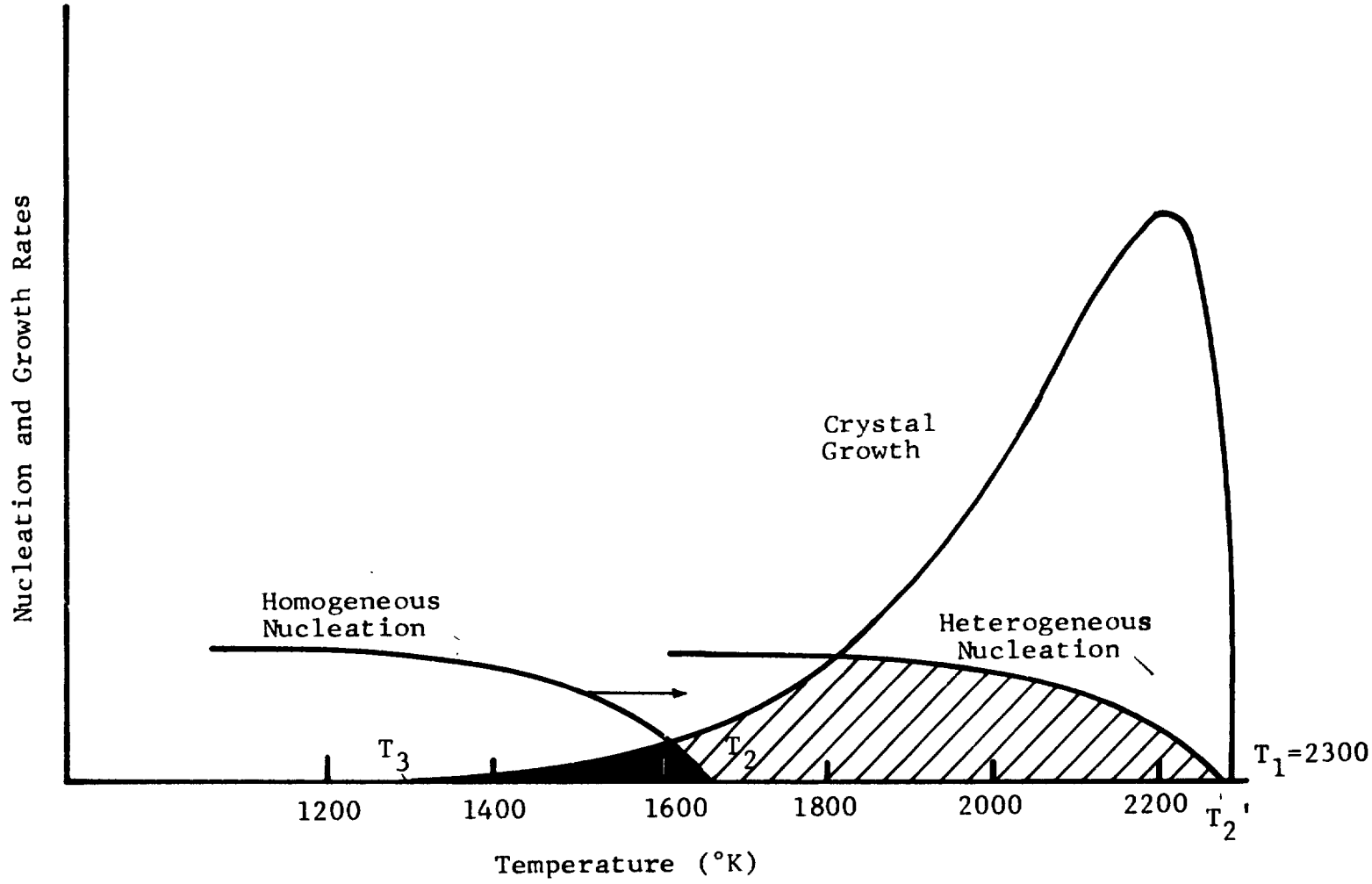

Figure 19 EFFECT OF HETEROGENEOUS NUCLEATION ON GLASS FORMING TENDENCY OF Al_2O_3

treatment of heterogeneous nucleation requires much information, such as the various surface energies discussed in Section 3.2, that is not readily available. Section 6.0 discusses an empirical approach that has been used to circumvent this problem.

4.5 Summary of Modeling Results for Single Component Systems

The kinetic and thermodynamic relationships describing glass formation that were developed in Section 3.0 have been applied to three relatively simple systems: 1) SiO_2, a well-characterized system, 2) B_2O_3, an excellent glass former, and 3) Al_2O_3, a material exhibiting no glass forming tendency based on empirical earth observation. It was found that viscosity, the viscosity-temperature relation, and the entropy of fusion are the parameters of prime importance in determining glass forming ability. For SiO_2 and B_2O_3, our analytical treatment predicted glass forming behavior that is consistent with the known behavior of these materials. For the Al_2O_3 system it was determined that the extrinsic effect of heterogeneous nucleation must be investigated in order to accurately predict the level of improvement in glass forming ability that could be obtained through in-space processing.

These results gave us confidence that we could now proceed to more complex systems covering more unique materials, and indicated to us the critical areas of investigation for such materials.

5.0 APPLICATION OF DERIVED KINETICS TO MORE COMPLEX SYSTEMS

The nucleation and growth kinetics that have been developed in Section 3.0 apply in general to single component substances or congruently melting (i.e., without composition change) compounds. The liquid-solid transformation process for these materials is termed non-reconstructive. No interatomic bonds within the participating molecules need be broken, and only short range diffusion processes are required for the transformation to occur at the liquid-crystal interface. In this instance, the molecular movements are treated as simply activated processes, with rate constants approximately equal to the coefficient of self-diffusion in the bulk liquid. This is convenient since the self-diffusion coefficient is related to the viscosity through the Stokes-Einstein equation, and viscosity data are more readily attainable kinetic data than diffusion data.

In multicomponent systems, however, the liquid to solid transformation often involves bond breaking and/or long-range diffusion processes, as discussed previously. In this instance the transformation is termed reconstructive. In network liquids, such as SiO_2, interatomic bonds must be broken in the network prior to molecular rearrangement. Since this bond breaking in network liquids must also precede viscous flow or self-diffusion, the free energy of activation for these processes will also be applicable as the kinetic barrier to the phase change process (25). Thus, in th. reconstructive transformation of a network liquid we can approximate the activation energy and the rate constant in the same manner as for non-reconstructive crystallization:

$$\Delta G' \text{ (nucleation)} = \Delta G'' \text{ (growth)} = \Delta G_a \text{ (flow activation energy)} \tag{48}$$

and,

$$D_n \cong D_g \cong D_s \cong \frac{kT}{3\pi a_o \eta} \tag{49}$$

However, in reconstructive crystallization where a large change in composition is involved, long range diffusion processes are required to bring the appropriate atomic species to the liquid-crystal interface. In this case the rate limiting step may be the diffusion of a particular (i.e., the slowest moving) species in the liquid matrix. In dealing with nucleation and growth kinetics and subsequent glass forming tendency of such materials, several methods have been postulated. Uhlmann and Chalmers (8) suggest that for nucleation involving large changes in composition that the kinetic barrier to nucleation, $\Delta G'$ in Equation (20), should be taken as the activation energy for diffusion of the slowest moving component in the matrix, and that the pre-exponential factor, $n\nu$, should be reduced by the mole fraction of the precipitating component. This presents a problem since the appropriate diffusion data are not as readily available as bulk liquid viscosity data. Furthermore, the kinetic term for nucleation, $\Delta G'$, is not necessarily equal to or even the same order of magnitude as the kinetic term for growth, $\Delta G''$ in Equation (32). This is due to the fact that growth is governed by atomic movements from a great distance from the interface, whereas the molecular movement involved in the nucleation process occurs relatively near the liquid-crystal interface. In general, growth in multicomponent systems where composition is a variable tends to be diffusion-controlled rather than interface-controlled. Hammel (4) has discussed the formulation for computing the volume fraction of material transformed for diffusion controlled growth:

$$v_f = \frac{8\pi}{15} S^3 D'^{3/2} I_o t^{5/2} \qquad (50)$$

where D' is the diffusion rate constant and S is a supersaturation term. Again, however, diffusion coefficients are required that are not readily available.

The question arises, then, of how we can predict the glass forming tendency in systems where diffusion controlled behavior is expected due to large compositional changes during the transformation, and for which the required diffusion data

are not available. Hillig (11, 26) has proposed that incorporation of a transient nucleation rate (5) will adequately account for long range diffusional effects that occur in a reconstructive transformation. Hammel (4) has applied transient nucleation analysis (Equations (26), (27), (28)) and diffusion controlled growth analysis (Equation 50)) to predict the volume fraction of cristobalite (SiO_2) precipitating from E glass ($13NaO_2 \cdot 11CaO \cdot 76SiO_2$) during cooling from the melt. In the nucleation rate expression Hammel used a value of X = .1 (mole fraction of precipitating phase in the melt, Equation (28)) to account for the long range molecular rearrangement. A value of X equal to unity is employed for a pure single component substance or a congruently melting compound. The determination of the appropriate value for X to use in a given reconstructive transformation is not clearly defined, however. Hammel (27) and Hillig (26) have proposed that X be determined by considerations of 1) what the expected rate-limiting species will be and 2) its concentration in the melt. In Hammel's treatment of diffusion controlled growth described above, a value of S in Equation (50) was determined using Frank's (28) tabulated values for diffusion controlled growth.

Unfortunately, the state-of-the-art in this nucleation-crystallization area has not reached the point where predicted transformation kinetics correlate well with reality in all instances. Especially in the case where large composition changes accompany the transformation, it may be that empirically derived nucleation and growth kinetics can be employed as discussed by Uhlmann (12). We have had the opportunity to investigate this. Section 6.0 describes how empirical evidence can be employed to describe glass forming tendency in a case where sufficient data is lacking to permit a purely analytical approach.

6.0 ANALYSIS OF COMPLEX SYSTEMS USING EMPIRICAL EVIDENCE

The homogeneous nucleation and growth kinetics that have been treated thus far apply generally to single component substances or congruently melting compounds, The last section discussed several possible methods of treating less ideal materials which undergo a composition change upon crystallization. However, even for simple substances we have found that a major problem exists in the manner in which we can handle the effects of heterogeneous nucleation. Referring to Section 3.2, we have shown that the analytical treatment of heterogeneous nucleation requires information about the magnitude of the solid-liquid, solid-impurity, and the liquid-impurity interfacial energies. This information is not readily available. Thus, analytical determination of the intrinsic glass forming ability and space candidacy of a material such as Al_2O_3 which is believed to crystallize via a heterogeneous nucleation mechanism, is a formidable task (See Section 4.4, The Al_2O_3 System).

For complex systems, i.e., systems for which our analytics are not entirely adequate, we now must rely, in part, on empirical evidence of the phase transformation process. The following section details how we have employed the empirical evidence available in a film of the crystallization of mullite to separate out heterogeneous nucleation, and determine the region of intrinsic glass formation. The empirical evidence mainly consisted of an indication of the viscosity-temperature relationship during the phase change process. Mullite was chosen for this analysis since to date it is the only material that such a film is available for. Ideal mullite ($3Al_2O_3 \cdot 2SiO_2$) crystallizes without composition change, so we can apply the same general kinetics that we have for single component systems.

It is our eventual aim to develop this analytical-empirical approach to the stage where it can be employed on even more complex materials. Once the mechanisms controlling the Earth-limited regions of glass formation in such unique materials have been determined, we can more readily assess how a technique such as

in-space processing can extend the boundaries of glass formation yielding technically improved products.

6.1 The Mullite System ($3Al_2O_3 \cdot 2SiO_2$)

Mullite glass has only been obtained (on earth) in very small quantities by splat cooling techniques. Our eventual aim is to determine a) the intrinsic glass forming region of mullite, b) the causes of the earth-observed poor glass forming ability of mullite, and c) whether or not a space-processing technique could be used to produce large mullite optical elements.

The glass forming tendency of the mullite ($3Al_2O_3 \cdot 2SiO_2$) system is indicated by the relative positions of the nucleation and growth kinetics, as discussed previously (i.e., T_2-T_3 region of simultaneous nucleation and growth). Unfortunately, an analytical treatment of nucleation and growth cannot be initiated until we have some basic kinetic and thermodynamic data for this system; mainly the heat of fusion (or the entropy of fusion) and the viscosity below the fusion temperature, Tm. An extensive literature search turned up neither the required entropy of fusion data, nor the required viscosity data. The only kinetic information we have for this system is 1) the fusion temperature, and 2) the viscosity at the fusion temperature. We do, however, have some empirical evidence of the crystallization of mullite: a filmed record of the air suspended laser melting and subsequent crystallization of mullite.* This empirical evidence of the phase change process gave us information regarding the temperature-viscosity relation where the process initiated, and led to the determination of the entropy of fusion of mullite. The information in the mullite crystallization film therefore plays an integral part in our determination of the glass forming behavior of mullite, as will become evident as we proceed through our analysis.

---

* Performed by R. A. Happe, North American Rockwell Corp., under NASA Contract NAS8-28991.

6.1.1 Determination of Critical Property Data

Our analysis starts with an estimation of the viscosity of glassy mullite. We have employed the same procedure we used when investigating the Al_2O_3 system: extrapolation of the viscosity below the liquidus temperature (i.e., Tm) by assuming the shape of the known SiO_2 η-T curve. Viscosity at the liquidus temperature was taken from Takamori and Roy[29]. The resultant viscosity relation is shown in Figure 20. It is emphasized here that this represents a first order approximation of the mullite viscosity. No attempt was made to consider arguments regarding the structural similarity between mullite and silica. Such more rigorous treatments of the viscosity of mullite below T_m based on available structure-viscosity theories will be considered later.

To proceed with our analysis we must now determine the entropy of fusion of mullite. This parameter was shown to be of prime importance in determining glass forming behavior. To derive this information we first need to have an estimate of the crystal growth rate of mullite. R. A. Happe analyzed films of the laser melting of mullite and presented overall growth rate data[30] for each experimental melt. The overall crystal growth rate (advancement of crystallization front) averaged for all experimental runs was

$$\mu \sim .776 \frac{cm}{sec} \sim 6x10^9 \frac{\text{Å}}{min}$$

For the purposes of our analysis we shall assume that this represents a peak growth rate, μ_p. (Refer to the shape of the μ-T relationship shown in Figure 8, for instance). This assumption is believed to be a valid first order approximation based on the following argument. Our previous work has shown that the peak growth rate of Al_2O_3 is $\sim 4x10^{10}$ Å/min. The liquidus temperature viscosity of alumina ($\sim$ 0.66 poise, reference 31) is a factor of 3.18 lower than that of mullite (2.1 poise, reference 29). It would thus be expected that the crystal growth rate of Al_2O_3 would be greater than that of mullite by roughly this factor. Multiplying the $6x10^9$ Å/min mullite growth rate by 3.18 gives $\sim 2x10^{10}$ Å/min for a rough estimation of the Al_2O_3 growth rate. This estimated

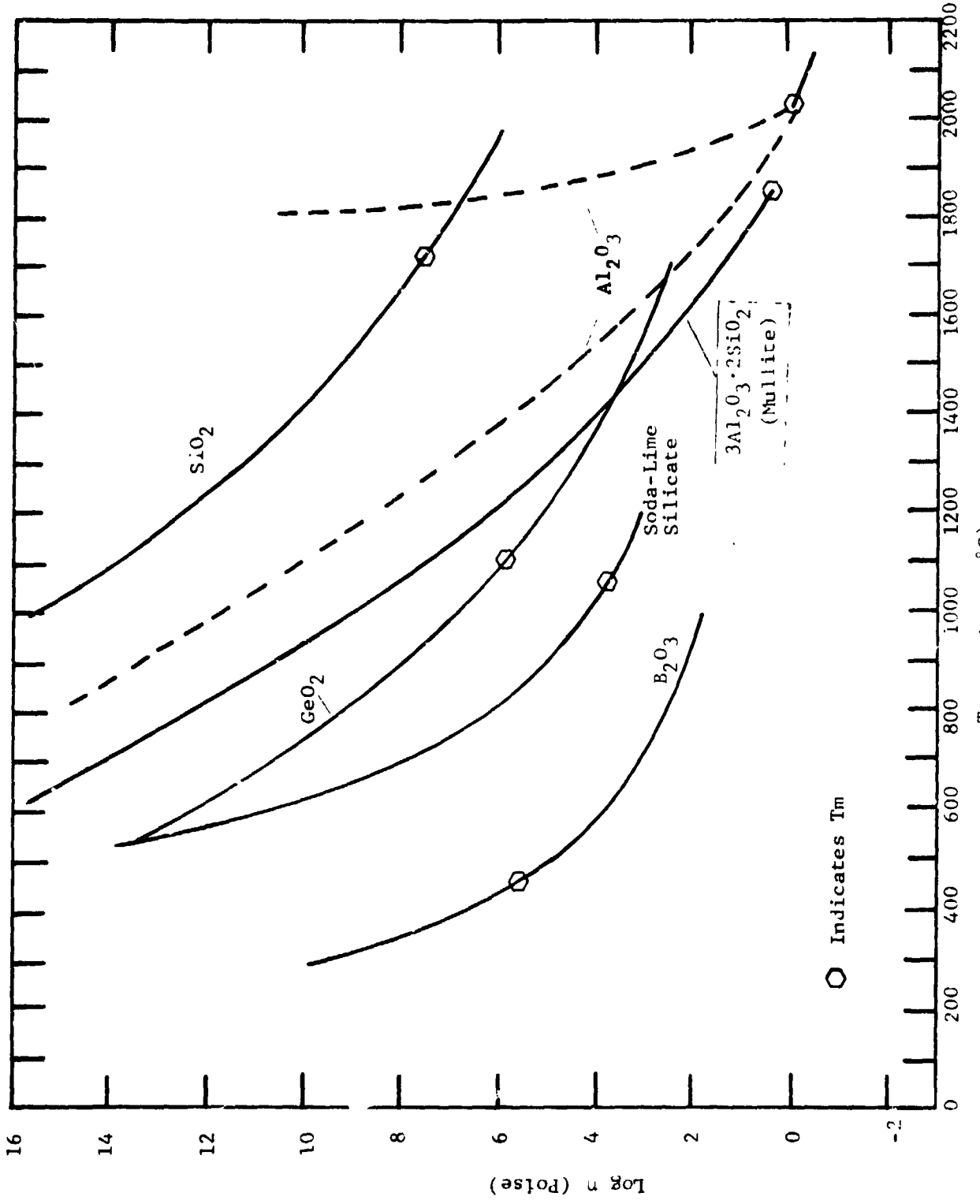

Figure 20 VISCOSITY FOR VARIOUS MATERIALS

growth rate for Al_2O_3, based on the mullite films, is within a factor of two of the Al_2O_3 growth rate we have computed from analytical considerations. Thus, the mean growth rate observed in the mullite laser melting films is quite close to the value for the peak growth rate.

Continuing our analysis, we now have a peak growth rate for mullite, and must now arrive at the temperature below T_m where mullite is expected to exhibit its maximum growth rate. A rough indication of this temperature is obtained by comparison with other systems. This comparison is based on observations made of the growth rate temperature dependence of the SiO_2, B_2O_3, and Al_2O_3 systems previously studied. In order to approximate growth rate temperature dependence, three temperatures are defined: T_m, T_p, and T_o. T_m is the thermodynamic fusion temperature, T_p is the temperature where the growth rate peaks at a maximum value, and T_o is the low-side temperature where the growth rate decays to a negligible magnitude. It was found that definite correlations exist for the temperature ratios T_o/T_m, T_o/T_p, and T_p/T_m for each of the systems studied, as shown in Table V. The data for these computations were extracted from the computed growth rate temperature curves for SiO_2, B_2O_3, and Al_2O_3 shown previously. Assuming that this correlation is valid for the mullite system, we now compute the temperature where mullite is expected to exhibit maximum growth:

$$T_p = .97(T_m) = .97(2123^oK) = 2059^oK \qquad (51)$$

The viscosity that glassy mullite would exhibit at this temperature (see Figure 20) is obtained graphically as $\eta = 6.3$ Poise at 2059^oK.

It is emphasized here that we are not aware of any theoretical basis for this correlation method for obtaining the approximate temperature where mullite will exhibit maximum crystal growth. In view of the lack of sufficient analytical or experimental data, however, this empirical/analogical approach is the only one that will allow us to go forward with the analysis. Our overall approach to describing the glass forming behavior of complex systems is an iterative one.

TABLE V

CORRELATIONS OF CRYSTAL GROWTH BEHAVIOR FOR THE Al_2O_3, B_2O_3, and SiC_2 SYSTEMS

Approximate Temperatures and Ratios (^oK)

Material	T_o	T_p	T_m	T_p/T_m	T_o/T_m	T_o/T_p
SiO_2	1600	1940	2000	.97	.8	.83
B_2O_3	620	700	725	.97	.85	.89
Al_2O_3	1980	2230	2300	.97	.86	.89

T_m = thermodynamic fusion temperature

T_p = temperature of peak growth rate

T_o = low-side temperature where the growth rate is $\sim$ zero (or $\mu << \mu$ peak, i.e., the tail of the curve)

If our final results are not compatible with experience and judgment, we go back and examine the credibility of the assumptions that have been made along the way.

Proceeding with our analysis, we can now evalute our analytical growth rate expression at the peak growth temperature (2059°K) to compute the only other unknown parameter for mullite, the molecular entropy of fusion. Assuming normal interface-controlled growth kinetics (3 to 2 mullite melts without composition change), the crystal growth rate expression is (see Section 3.3.1.1):

$$\mu = \frac{fkT}{3\pi a_o^2 \eta}\left[1 - \exp\left(\frac{-\Delta s_f \Delta T}{RT}\right)\right] \qquad (52)$$

The pertinent parameters are:

$\mu = .776 \frac{cm}{sec}$ (growth rate from mullite film)

$T_m = 2123^oK$

$T = 2059^oK$ (Temp. where $\mu = \mu$ peak)

$f = 1$ (congruent melting)

$a_o = 2.5\text{Å}$ (assumed)

$\eta = 6.3$ poise at 2059^oK (see Figure 20) = $15.06 \times 10^8 \frac{cal\ sec}{cm^3}$

$R = 1.987$ cal/mole^oK (gas constant)

$\Delta T = T_m - T = 64^oK$

$k = 3.3 \times 10^{-24}$ cal/^oK (Boltzman's constant)

These values were substituted into Equation (52) to evaluate the entropy of fusion, Δs_f, for mullite:

$$\Delta s_f = 6.78 \frac{cal}{mole^oK} \qquad (53)$$

The heat of fusion of mullite is calculated to be:

$$\Delta h_f = \Delta s_f T_m = 14{,}400 \frac{cal}{mole} \qquad (54)$$

These computed thermodynamic parameters for mullite agree well with values derived from estimates of the heat of fusion and entropy of fusion based on weighted averages of the mole constituents (references 32 and 33):

$$\frac{3}{5}(Al_2O_3) + \frac{2}{5}(SiO_2) = \text{mullite}$$

$$.6(\Delta h_{f/Al_2O_3}) + .4(\Delta h_{f(SiO_2)} =$$

$$.6(26,000) + .4(2000) = 16,400 \frac{cal}{mole}$$

$$\text{or } \Delta h_f(\text{mullite}) = 16,400 \frac{cal}{mole}$$

and thus

$$\Delta s_f(\text{mullite}) = \frac{16,400}{2123} \tilde{=} 7.7 \frac{cal}{mole^oK}$$

Thus, the value of the entropy of fusion of mullite we have computed from the empirical results of laser melting experiments is within roughly 10% of the value computed from a first order approximation.

6.1.2 Nucleation and Growth Kinetics

We have thus far determined an approximate viscosity-temperature relationship for vitreous mullite, and utilized the films of the laser melting/crystallization of mullite to derive an approximate value for the entropy of fusion. With this thermodynamic and kinetic information we can now proceed to analytically describe the glass forming tendency of mullite. This is done by obtaining a rough idea of the region of simultaneous nucleation (homogeneous) and crystal growth for this system.

For our initial analysis of this system we need only investigate steady state nucleation behavior. We have shown previously that for the congruent melting of the $3Al_2O_3 \cdot 2SiO_2$ system, the steady state homogeneous nucleation rate is given by the expression:

$$I_o = \frac{nkT}{3\pi a_o^3 \eta} \exp\left[\frac{-16\pi}{3} \frac{\Delta s_f T_m^3}{R\alpha^3 T \Delta T^2}\right] \quad (55)$$

For the mullite system the following materials parameters apply:

Δs_f = 6.77 cal mole^{-1} K^{-1}
α = 2, 2.5, 3 (variable)
T_m = 2125°K
a_o = 2.5 Å (assumed)
$\eta(T)$= See Figure 20
n,k,R = Constants

These values were inserted into Equation (55) and the steady state homogeneous nucleation rate for mullite computed and plotted as illustrated in Figure 21 (for variable α).

The crystal growth rate for mullite (normal interface controlled growth being assumed) is given by the expression

$$\mu = \frac{fkT}{3\pi a_o^2 \eta} \left[1 - \exp \frac{-\Delta s_f \Delta T}{RT}\right] \qquad (56)$$

The pertinent material parameters (given above, with f equal to unity) were inserted in this relation, with the resultant growth velocity-temperature curve shown in Figure 22. The extremely large theoretical growth rates shown for mullite (up to 6×10^9 Å/min) are the result of the low liquidus temperature viscosity (see Figure 20).

Superimposing the homogeneous nucleation and growth rate behavior of mullite on the same temperature scale will indicate the "T_2-T_3" region of simultaneous nucleation and growth (i.e., a qualitative indication of intrinsic glass forming tendency). This is illustrated in Figure 23, where for convenience the growth velocity is expressed as log μ. It is observed that if the α parameter for mullite lies somewhere in the range $2.5 \leq \alpha \leq 3$ (reasonable values), then it would be expected that mullite would intrinsically nucleate and crystallize upon cooling from the melt at a temperature between $\sim$ 1500°K and 1700°K, and would continue to undergo the liquid-solid transformation down to a temperature $\sim$ 1200°K. Thus, in the absence of nucleating heterogeneities

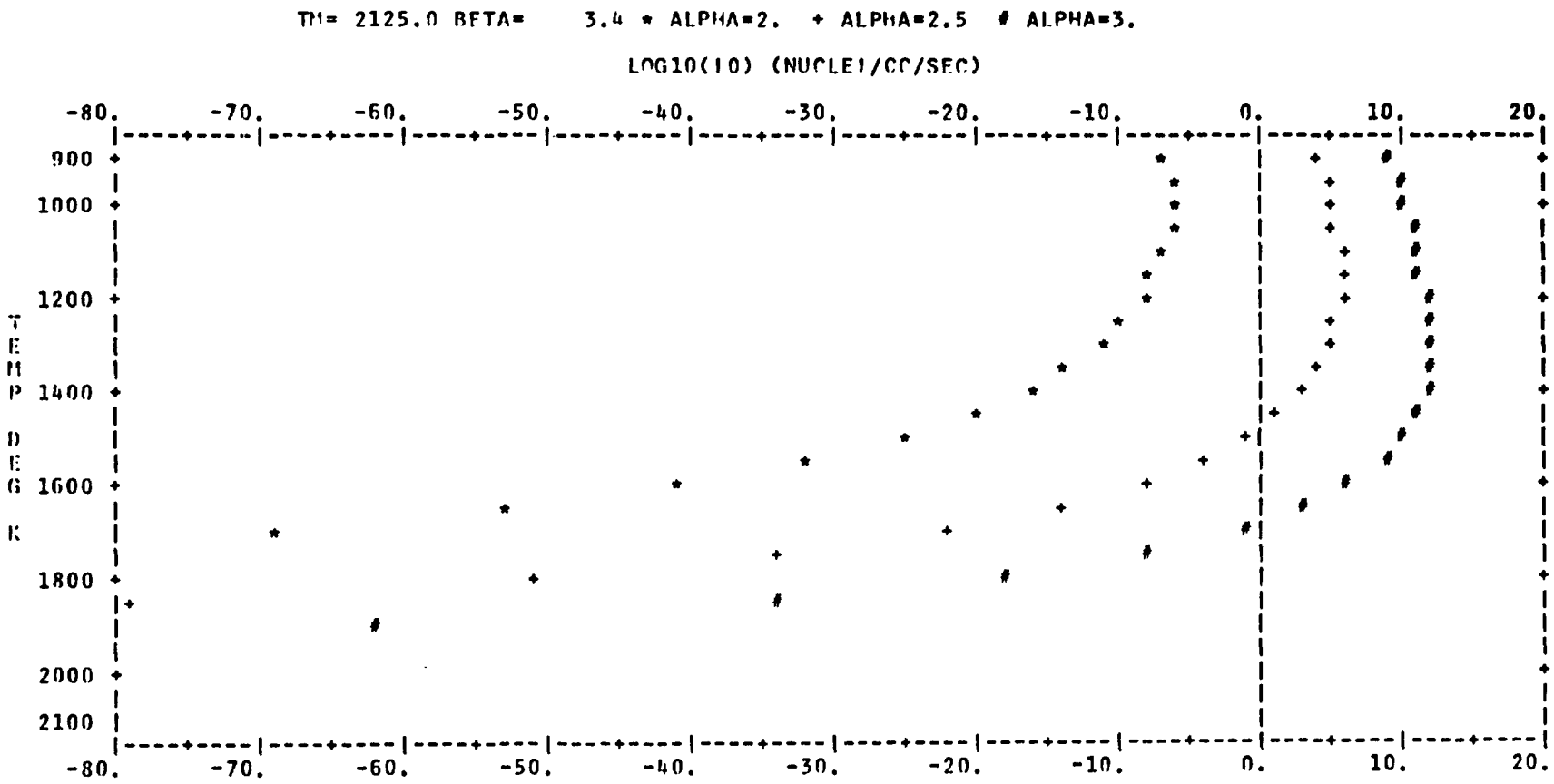

Figure 21. Nucleation Rate for Mullite as a Function of Alpha (Steady State)

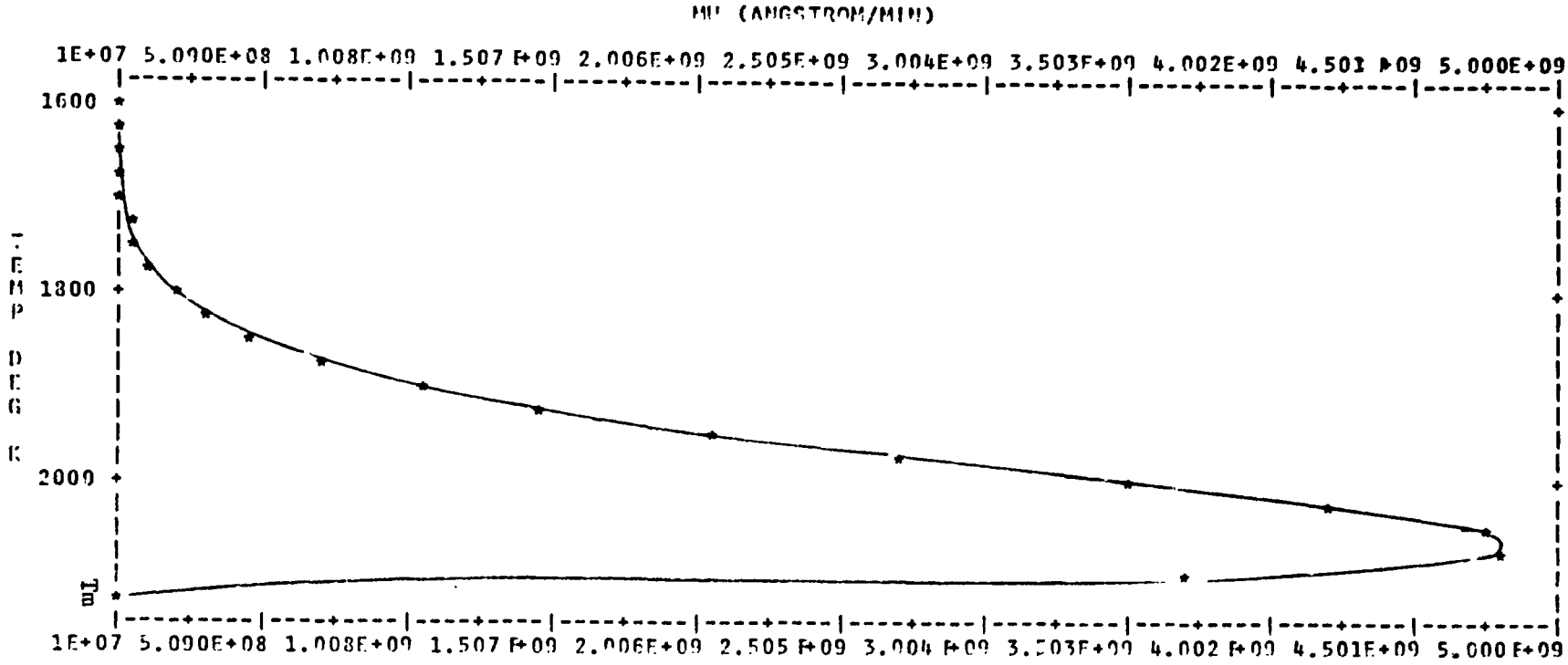

Figure 22. Crystal Growth Rate (Mullite)

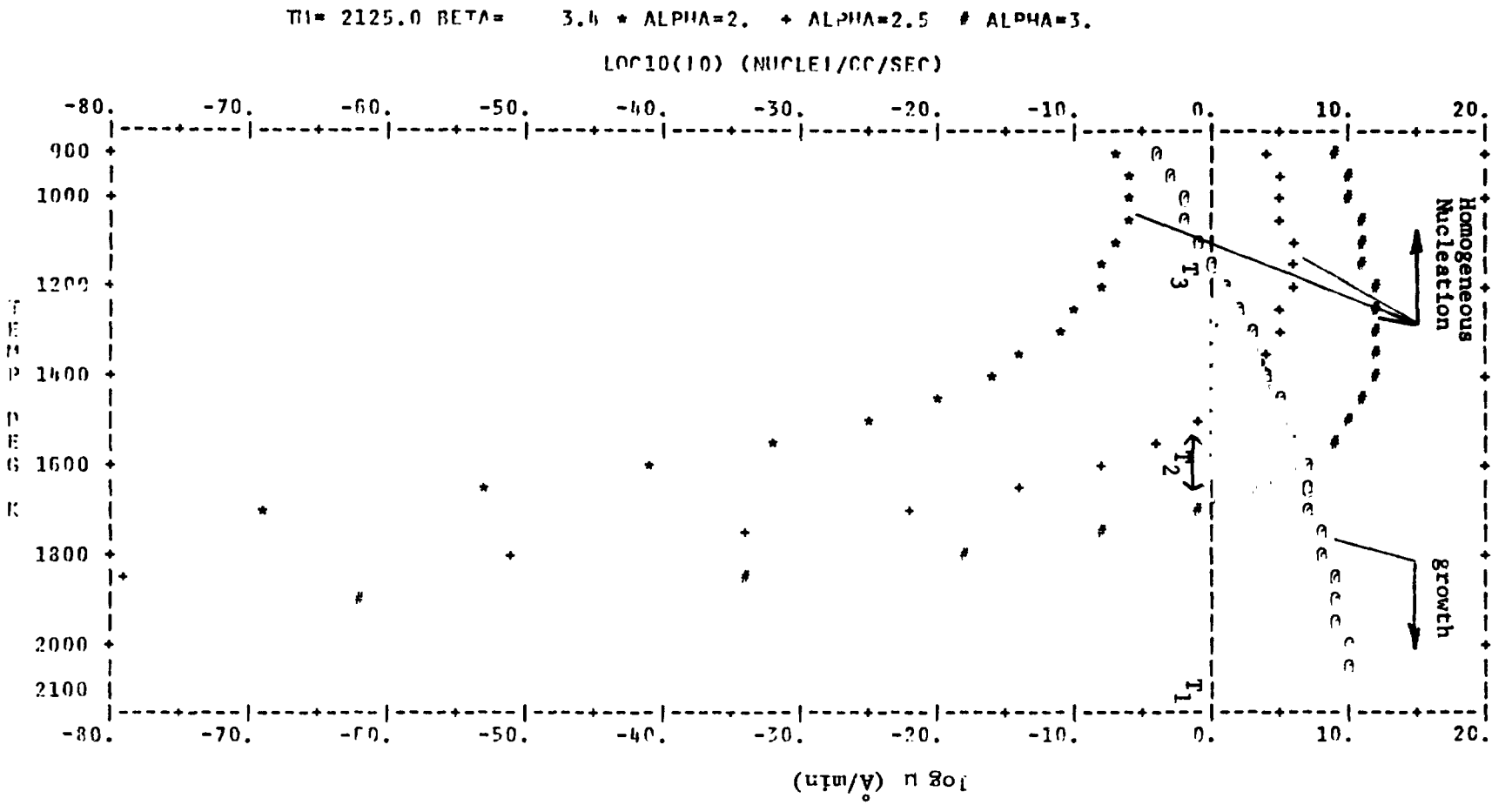

Figure 23. Intrinsic Nucleation and Growth Characteristics for Mullite
(Shaded region = simultaneous nucleation and growth)

the temperature region of roughly 1700°K-1200°K would have to be passed through rapidly to form glassy mullite (i.e., avoid detectable crystallization).

In practice, however, it is a common laboratory occurrence that mullite crystallizes immediately upon passing the liquidus temperature (thermodynamic fusion temperature, T_m). The crystallization of mullite can be routinely observed at undercooling temperatures (i.e., degrees below T_m) much less than the $\sim 400^{\circ}K$ undercooling predicted in Figure 23 (i.e., $T_1-T_2 = 400^{\circ}K$) for homogeneous nucleation (i.e., intrinsic glass formation). This is the result of nucleating heterogeneities which tend to shift the nucleation curve, i.e., T_2, closer to $T_1 = T_m$. Heterogeneous nucleation is the process by which the liquid-solid phase transformation is initiated by foreign surfaces present in the liquid such as container wall asperities or insoluble particles. These surfaces tend to reduce the barrier to nucleation represented by the surface energy between the liquid and solid phases. As a result of these extrinsic parameters the critical embryo size is reduced and the supercooling temperature is raised (the supercooling temperature is the temperature where the first detectable nucleation is observed upon cooling from the melt).

This discrepancy between our analytical results and general experience for the mullite system was also observed in our analysis of Al_2O_3 (refer to Section 4.4). However, for mullite the laser melting films provide a unique way of dealing with heterogeneous nucleation in the absence of the required analytical data. This will be discussed in the following section.

6.1.3 Treatment of Heterogeneous Nucleation

The air suspended/laser melting experiments provide a convenient means of investigating the heterogeneous nucleation effect. In the actual laser melting of mullite performed by R. A. Happe, several phenomena were observed or recorded. We have reviewed films of this experiment at IITRI and have observed two important phenomena. First, crystallization of the mullite sphere proceeded from a finite number of nucleation sites (from one to three).

Second, the nucleation and initial crystallization appeared to occur on the surface of the mullite sphere. This was discernible as a contoured crystallized surface observed while the mullite sphere was rotating. These phenomena indicate that the nucleation was heterogeneous, not homogeneous.

The following argument supports our contention that since only one to three sites were observed, the nucleation had to have been caused by a heterogeneous mechanism. From the observed rate of advancement of the crystallization front, ($\sim$ .7 cm/sec) and the sample size ($\sim$ .6 cm diameter), the total time elapsed for the process was on the order of 0.5 sec. The cooling rate for the experiment was estimated by Happe to be $\sim$ 100°C/sec. Thus, during the observed transformation the temperature decreased roughly 50°C. Assuming a uniform temperature distribution and referring to the mullite nucleation rate shown in Figure 21, it is illustrated that if the nucleation process were homogeneous, then roughly 10^2-10^3 sites would have nucleated. During the process only 1 to 3 sites were observed, supporting the heterogeneous nucleation hypothesis.

R. A. Happe's analysis of the mullite films and the actual melting experiments provide additional information[34,35] about the crystallization behavior of mullite: 1) an undetermined amount of initial superheating above T_m was employed in all experiments, 2) a temperature drop of 600°C to 1000°C was observed from the initial superheated condition to the point where crystallization was first visually detected, and 3) before and during crystallization the viscosity of the sample appeared low and did not rapidly change with decreasing temperature. The latter item was inferred from the observed rapid oscillating motion, "jiggling," of the mullite sphere.

Using this information about the freezing of mullite, we will attempt to describe the experiments shown in the mullite films analytically. The idea here is to see how intrinsic the glass formation was with the aim of eventually being able to predict how we can conduct an experiment in space that will yield a glass that cannot be produced on Earth.

One of the most basic parameters of glass forming ability is the temperature T_2 where the first detectable phase change is observed upon cooling from the melt. If the crystallization of mullite observed in the films were produced by intrinsic homogeneous nucleation, then the temperature at which the first detectable phase change would be detected (upon cooling from the melt) would be $\sim 1700^{o}K$ (T_2 in Figure 23). Figure 20 indicates that the viscosity of amorphous mullite at $1700^{o}K$ would be $\sim 1 \times 10^{4}$ Poise. This level of viscosity is believed to be too high to produce the "jiggling" observed in the mullite films. A viscosity of 10^{4} Poise is inconsistent, we believe, with R. A. Happe's observations that at the time of initial crystallization, the viscosity was very low, and did not increase significantly with decreasing temperature. A viscosity of 10^{4}Poise is three orders of magnitude greater than the liquidus temperature viscosity. Therefore, the viscosity of the mullite in the films just prior to crystallization must have been much lower than 10^{4} Poise, say, in the range of $\sim 10^{1}$ Poise. This means that the temperature of initial detectable crystallization would have to have been roughly $1900^{o}K$ (from Figure 20, $\eta = 10^{1}$ Poise at $\sim 1700^{o}C$). Thus temperature T_2 in the actual melting experiment would be $1900^{o}K$, rather than $1700^{o}K$ as predicted by Figure 23 for the case of homogeneous nucleation.

Shifting the initial crystallization temperature T_2 upwards to $1900^{o}K$ shows the effect of heterogeneous nucleation. This is illustrated in Figure 24. The nucleation curve is shifted from T_2 to T_2', closer to the fusion temperature $T_m = T_1$. This evidence for heterogeneous nucleation correlates with our observations that nucleation appeared to initiate at a finite number of locations on the mullite surface.

If, then, the initial crystallization occurred at approximately $1900^{o}K$ (T_2'), the amount of undercooling becomes $T_m - T_2' \cong 200^{o}K$. Therefore, the amount of superheating in these experiments would be in the range of 400^{o} to $800^{o}K$ above the liquidus temperature T_m ($\sim 2100^{o}K$).

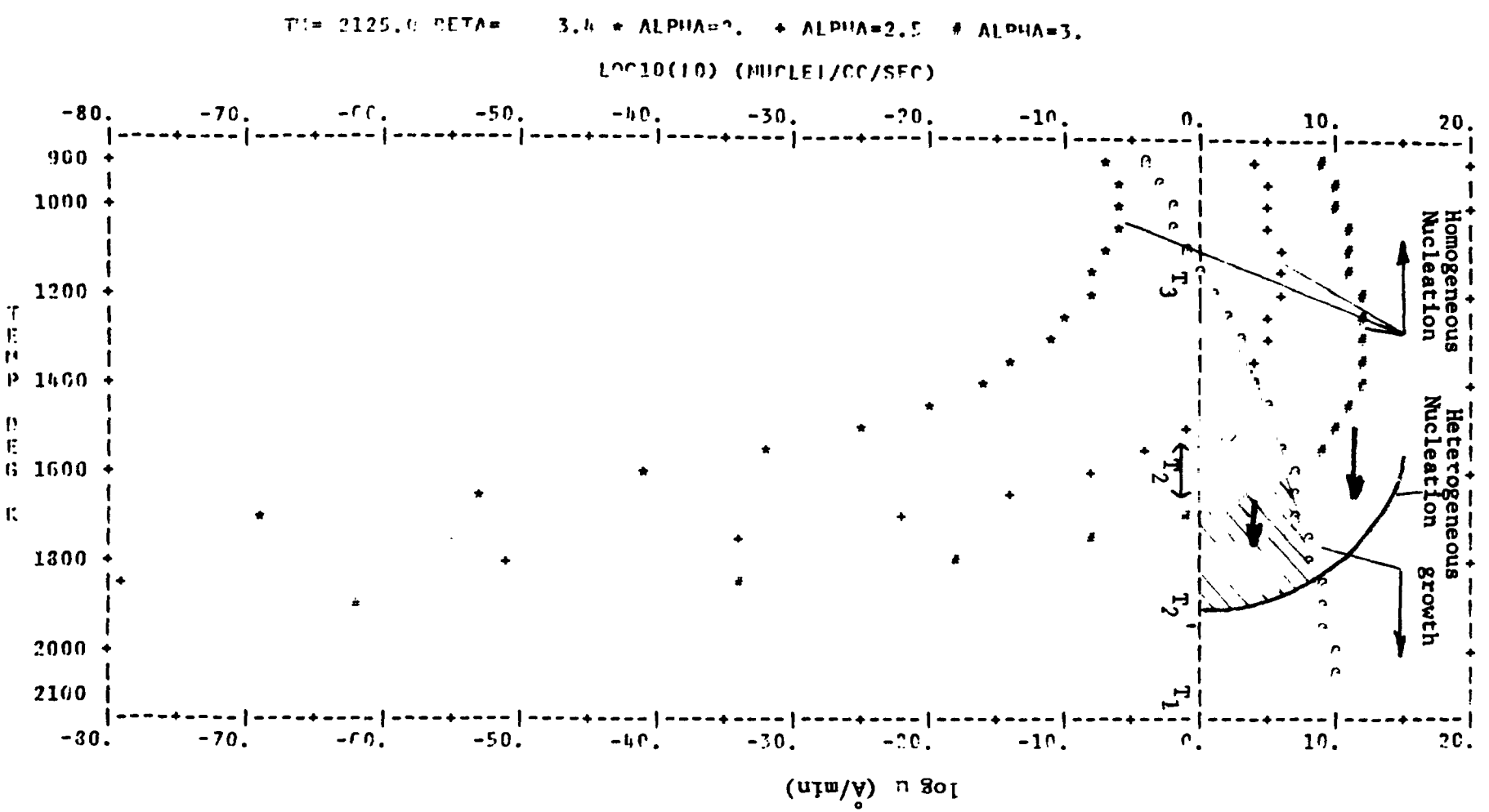

Figure 24. Nucleation and Growth Characteristics for Mullite Showing effect of Heterogeneous Nucleation Observed in Rockwell Films

This is based on R. A. Happe's observations that the mullite temperature dropped from 600° to 1000°C from the time the laser was shut off until crystallization was first detected visually.

6.1.4 Critical Cooling Rates

For the intrinsic case of homogeneous nucleation, our first-order approximation analysis has shown that when slow cooled from the melt ($T_1 = T_m = 2125^{\circ}K$), one would expect to observe the liquid-solid phase transormation when the temperature reached the 1500° to 1700°K level, depending on whether the α parameter is closer to 2.5 or 3.0 (see range of T_2 indicated in Figure 23). The laser melting films were interpreted to estimate that for the actual crystallization observed by Happe, the first detectable phase transformation occurred at roughly 1900°K. This illustrates the effect of heterogeneous nucleation sites, and shifts the nucleation curve upwards from T_2 to T_2' as shown in Figure 24.

We now attempt to quantify these cases by computing the cooling rate required to avoid detectable phase transformation. Using Uhlmann's procedure [13], which was discussed in Section 3.4, computer software was developed to perform this analysis. A typical computer-generated time-temperature-transformation curve is illustrated in Figure 25.

The first set of computations of critical cooling rates assumed that $\alpha = 2.5$, as shown in Figure 26. The critical cooling rate for glass formation was computed for three cases: (A) for homogeneous nucleation, i.e., intrinsic behavior, (B) for nucleation that is heterogeneous to the extent that we have previously estimated the laser melting experiments to be (i.e., T_2 shifted upwards to $T_2' = 1900^{\circ}K$), and (C) for nucleation that is heterogeneous to the extent that might be present in conventional earth melting experiments (i.e., T_2 shifted upwards to $T_2' \sim 2100^{\circ}K$, which corresponds to nucleation just below the fusion temperature (2125°K) from a site such as a crucible wall or an undissolved refractory impurity particle). These three cases are illustrated in the "T_2-T_3" region plot shown in Figure 26. Figure 27 illustrates these three cases repeated for the case where $\alpha = 3.0$.

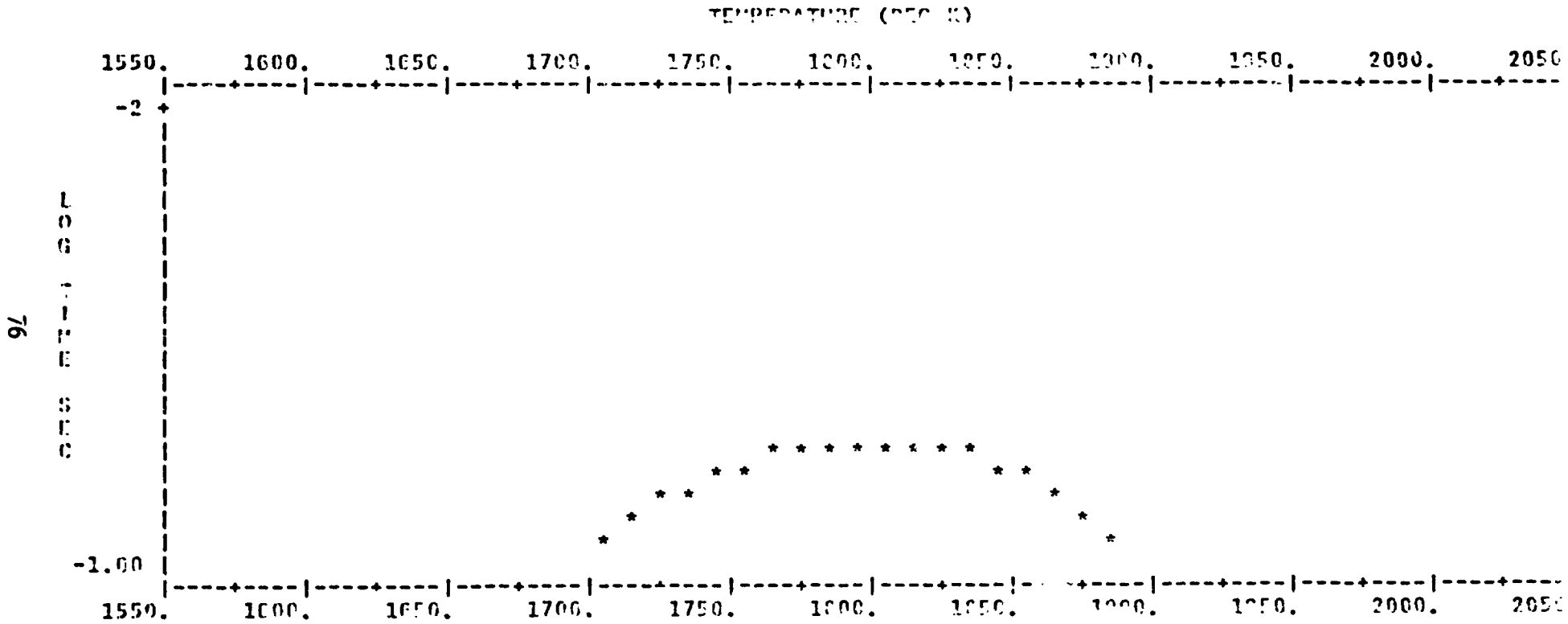

Figure 25. Computer Generated Time-Temperature-Transformation Curve

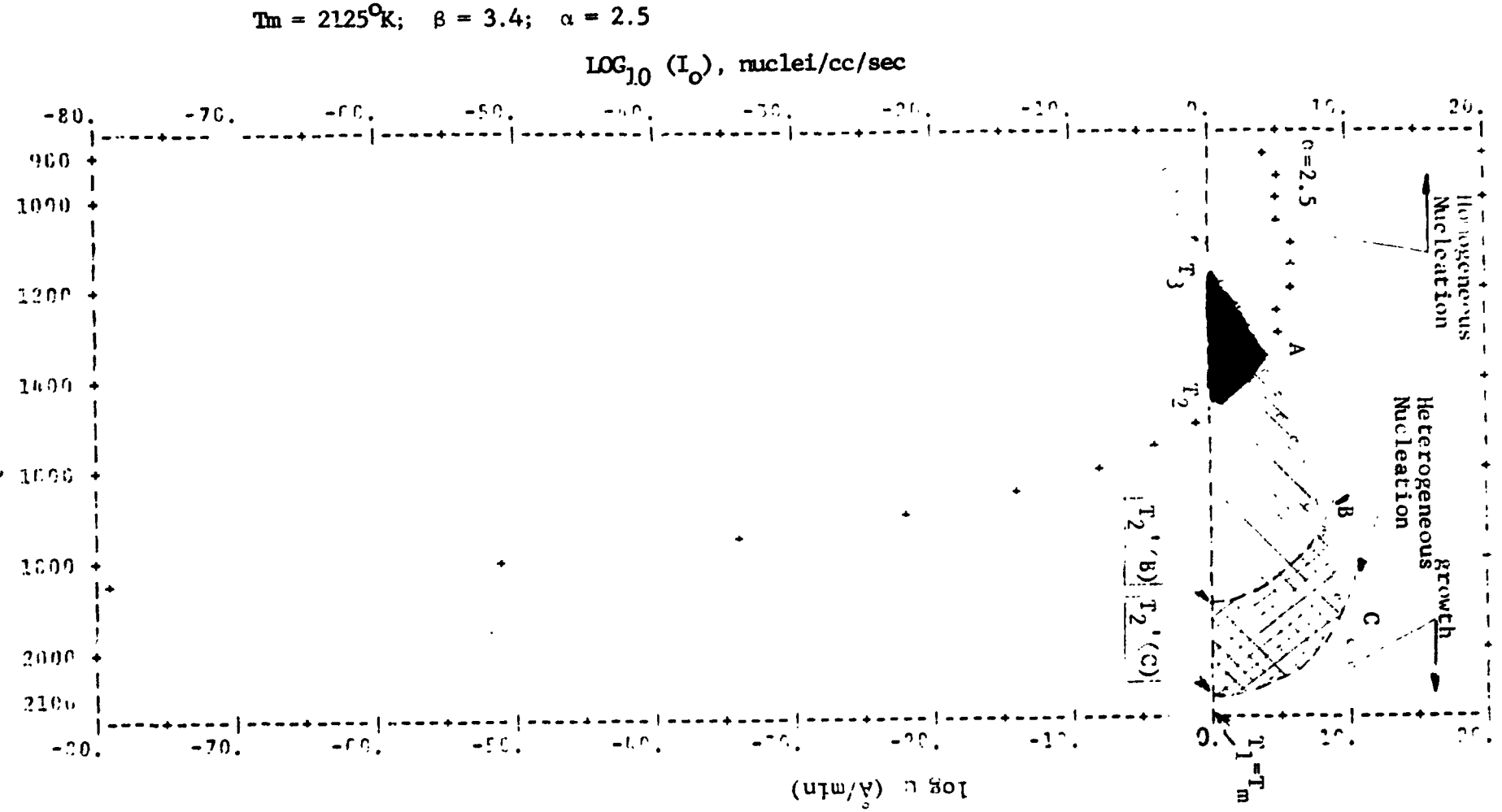

Figure 26. Extrinsic and Intrinsic Nucleation and Growth Characteristics for Mullite (α=2.5) (Shaded region = simultaneous nucleation and growth)

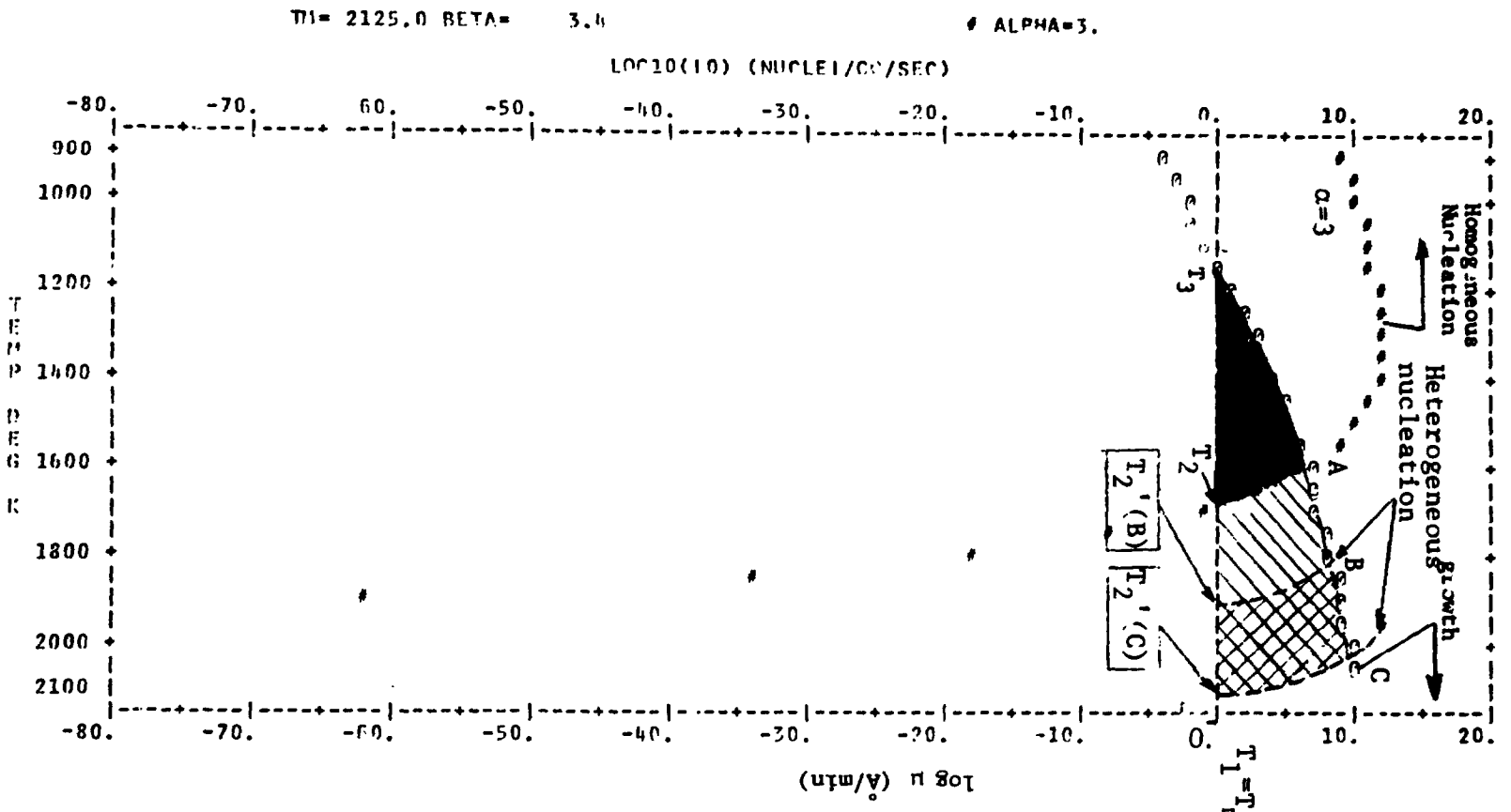

Figure 27. Nucleation and Growth Characteristics for Mullite (α=3) Extrinsic and Intrinsic
(Shaded region = simultaneous nucleation and growth)

The results of this analysis are presented in Table VI. The 10^4-10^5°K/sec critical cooling rate predicted for a "conventional" Earth-bound experiment seems reasonable since "splat" techniques have been found to be the only methods capable of producing significant glassy mullite phases[29,36] on Earth. Quench rates of 10^5-10^6°K/sec are estimated for splat cooling methods.

The cooling rate of 10^3-10^4°K/sec that we have predicted to be critical for the conditions under which the laser melting of mullite was performed also appears reasonable. This is evidenced by the fact that glassy mullite was not produced in these experiments, where the experimental cooling rate was estimated to be only $\sim 10^2$°K/sec[37].

The computed critical cooling rate for mullite free of nucleating heterogeneities is 10^1-10^3°K/sec, as shown in Table VI. Conventional quenching methods such as radiation cooling lie within this region. Therefore, according to this analysis, mullite has intrinsic glass-forming qualities realizable through relatively conventional quenching methods. Achieving intrinsic glass formation thus becomes a problem of eliminating heterogeneous nucleation sites. This can be partially accomplished by going to containerless space processing where no sample-crucible interface exists that would provide heterogeneous sites.

6.1.5 Summary of Mullite Analysis

To circumvent the problem of the lack of kinetic data for the complex mullite system, the empirical evidence of the phase transformation process available in the North American Rockwell films was utilized. Our conclusions regarding the laser melting experiments and the glass forming ability of mullite, derived from our "T_2-T_3" region nucleation and growth analysis are as follows:

- the liquid-solid transformation observed in the films initiated by a heterogeneous nucleation mechanism. This was deduced from the fact that crystallization initiated on the surface of the sample sphere from a finite number

TABLE VI

COMPUTED CRITICAL COOLING RATES FOR MULLITE ($^{o}K\ sec^{-1}$)

	Intrinsic	Estimated for Rockwell Laser Melting Experiments	"Conventional" Earth-Bound Experiment
α-parameter	Homogeneous T_2*	Heterogeneous T_2' ~1900°K	Heterogeneous T_2' ~2100°K
2.5	10^1	6×10^3	3×10^4
3.0	4×10^3	6×10^4	5×10^5

* T_2 ~ 1475°K for α = 2.5

  T_2 ~ 1725°K for α = 3.0

of sites. If the nucleation were homogeneous, the entire sphere volume would have nucleated simultaneously.

- the first detectable crystallization occurred at a temperature level, T_2' of $\sim 1900^oK$ (i.e., at an undercooling of $\sim 200^oK$). This was deduced from the observations of R. A. Happe that at the time of initial visually detectable crystallization, the mullite sphere exhibited a "jiggling" motion. Such motion would be produced by a material with a viscosity of $\sim 10^1$ poise, corresponding to a temperature of 1900^oK for mullite.
- an initial superheating of $\sim 400^oK$ existed in the laser melting experiments. This was computed from Happe's estimate of the degree of cooling obtained after laser shut down to the first detectable phase change, together with the estimated temperature T_2'.
- the cooling rate for the laser melting of mullite was $\sim 10^{2o}K/sec$ (derived from the cooling curves shown by Happe).
- for the amount of heterogeneous nucleation existing in the laser melting experiment, a cooling rate of 10^3 to $10^{4o}K/sec$ would be necessary for glass formation. This result was computed from IITRI's analysis, and is consistent with the estimated cooling rates of these experiments. and the fact that mullite glass was not obtained.
- for the amount of heterogeneous nucleation present if a crucible were used or if no superheating were used, a cooling rate of $\sim 10^{5o}K/sec$ would be required for glass formation. This result was computed from IITRI's analysis, and is consistent with the known cooling rates of splat cooling techniques ($\sim 10^5$-$10^{6o}K/sec$), and the fact that significant glassy mullite phases have only been obtained using splat techniques.

- a cooling rate of 10^1 to 10^3°K/sec will be necessary for glass formation in the mullite system if all heterogeneous nucleation sites are eliminated (represents the intrinsic behavior of mullite, computed from IITRI's analysis). The cooling rate required for intrinsic glass formation in mullite is within the range of relatively conventional quenching techniques such as radiation cooling.

This first order approximation analysis has indicated that if a technique such as weightless, containerless space processing could be utilized to remove all heterogeneous nucleation sites from mullite, then mullite glasses which are relatively unobtainable on earth could be produced. The potential exists for relatively large optical elements since conventional cooling methods could be employed.

It is emphasized here that this analysis has given us a first order approximation of cooling rates critical for glass formation. Enough evidence has been presented, we believe, to warrant further consideration of mullite as a space processing candidate material. However, several refinements to our analytical technique should eventually be considered. First, transient nucleation has not been considered in this analysis. We have only included I_o, the steady state nucleation rate. Secondly, when we shifted the nucleation curve upwards to simulate the existence of heterogeneous nucleation sites, the shape of the nucleation-temperature curve was not changed. This mainly involves not accounting for changes in the shape of the viscosity-temperature curve at different temperature levels. Finally, considerations should be given to theoretical viscosity-structure relationships to improve upon the extrapolation technique used to estimate mullite viscosity below the fusion temperature. Nonetheless, the present analysis has exhibited sufficient correlation with empirical observations to be of value in predicting the range of cooling rates necessary for intrinsic glass formation. Further discussion of possible refinements to our analysis is presented in Section 7.0.

6.2 Additional Experiments - Calcium Aluminate Glasses

In addition to the mullite work described above, various calcium aluminate compositions were investigated. High alumina calcium aluminate has possible ir-transmission applications, but it is not a good glass former based on earth-bound experience. It is our eventual aim to determine if space processing could be utilized to extend the regions of glass formation for this material.

The $xCaO \cdot yAl_2O_3$ compositions for this study were prepared by reaction sintering of a cold pressed precursor. The precursor materials were calcium carbonate and aluminum tri-hydrate. The general reaction equation is:

$$xCaCO_3 + y\left[Al_2O_3 \cdot 3H_2O\right] \rightarrow xCaO \cdot yAl_2O_3 + xCO_2\uparrow + 3yH_2O\uparrow \quad (57)$$

The phase diagram for this system and the earth-determined glass forming region are illustrated in Figure 28. Particular compositions for our study lie within the glass forming region and on the high-alumina side of the glass forming region - as designated by #1, #2, etc.

Referring to Figure 28, compositions #1 and #2 (i.e., 50w/o alumina and 70 w/o alumina, respectively) were prepared at IITRI and then air suspended and laser-melted at Rockwell Corp. The good glass forming tendency of a 50 w/o Al_2O_3 composition was confirmed in the laser melting experiment[39]. Additionally, the 70 w/o alumina composition was also found to exhibit glass formation[40]. This is significant since this composition lies outside the previously accepted glass forming region shown in Figure 28.

The scheduling of the preparation of the 75 w/o and 80 w/o alumina samples at IITRI was not compatible with the time schedules of the Rockwell program. In the future, we intend to prepare the 75 w/o and 80 w/o alumina systems. After sintering at roughly 1600°C the existence of the desired $Al_2O_3 + 3CaO \cdot 5Al_2O_3$ material (See Figure 29) will be verified by X-ray diffraction. The sample will then be sent to R. A. Happe for subsequent laser melting.

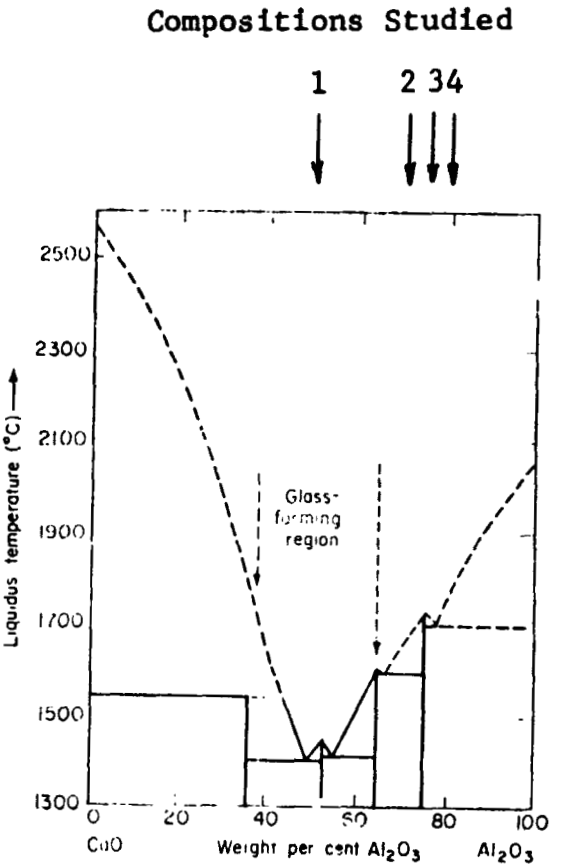

Figure 28. The Glass Forming Region in Relation to the Phase Diagram for the Calcium Aluminate System (38)

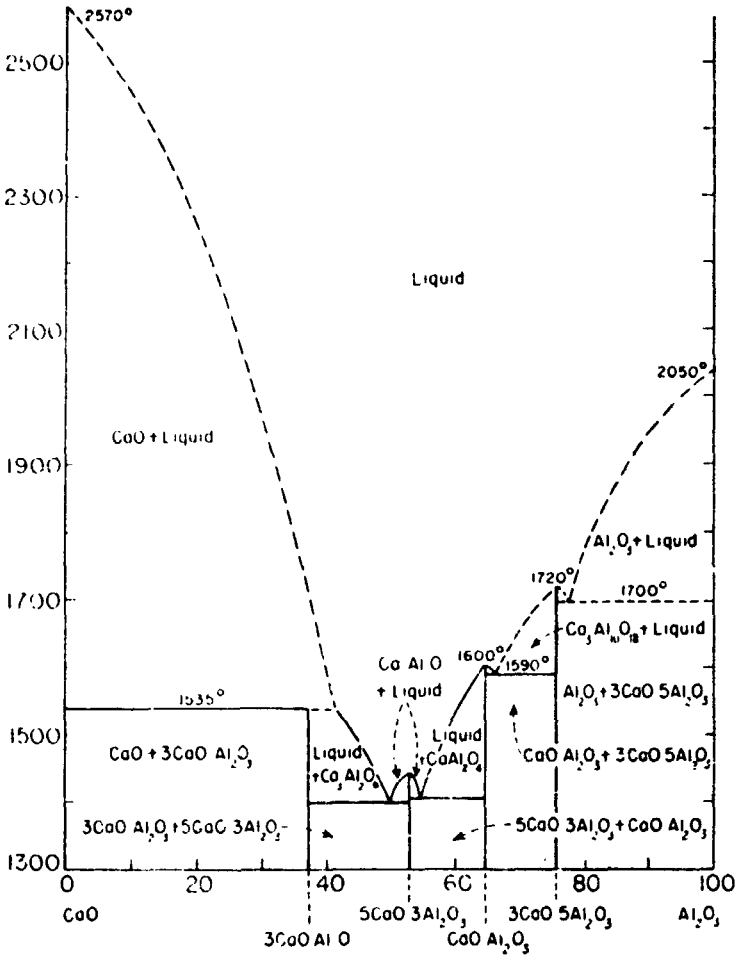

Figure 29. CaO--Al_2O_3 Phase Diagram (41)

Eventually, the alumina content of the IITRI-supplied calcium aluminate samples will become high enough that good quality glass will not be obtained in the laser melting experiments. At that point, we can apply our analytical nucleation and crystallization relationships to the films of the crystallization phenomena as we have done for the mullite system. When this work is completed the results will be reported to NASA in the form of supplementary information. In this manner, the intrinsic glass forming ability can be determined, and the candidacy of the particular calcium aluminate composition can be assessed.

7.0 SUGGESTIONS FOR FUTURE WORK

IITRI's suggestions for future work in this area entail 1) refinements in the analytical techniques for unique materials, and 2) the assessment of space processing candidacy through controlled experiments and analysis.

7.1 Improvements in Analytical/Empirical Techniques

Improvements in our analytical-empirical prediction techniques can be derived from a continued cooperative effort between IITRI and North Americal Rockwell Corporation. Rockwell's part would be the laser melting of various oxide materials. IITRI's part would be theoretical and analytical work leading to a quantitative description of the glass forming ability of the oxides studied.

R. A. Happe has indicated[42] that in Rockwell's continuing program, "Manufacturing Unique Glasses in Space" (NAS8-28991), filming of the laser melting of six materials (V_2O_5, GeO_2, Nb_2O_5, CoO, Al_2O_3, and Y_2O_3) will be produced in a cooperative effort by Rockwell and Sandia Corporation. The purpose of these experiments will be to develop a densitometric film analysis technique for determining the temperature of the sample during the liquid-solid phase transformation.

In IITRI's analysis of the glass forming ability of the mullite system on the current program, such a temperature-time history during the filmed laser melting experiment was not available. Consequently, the required kinetic data had to be derived by either a) extrapolation, as for the viscosity-temperature relation below the fusion temperature, or b) by deductive reasoning, as in the instance where we estimated the temperature where Happe observed the first detectable phase transformation in the mullite films. In the latter instance, "jiggling" of the cooling mullite sphere was observed during much of the crystallization process. The approximate viscosity that would be consistent with such a motion was estimated, thus leading to an estimated temperature

at which the event occurred. This analysis, although approximate, led to critical cooling rates for glass formation that are compatible with empirical evidence (refer to Section 6.1).

However, the cooperative Rockwell-Sandia effort to obtain an accurate temperature-time history during the laser melting experiments offers a unique opportunity for removing some of the assumptions and approximations in IITRI's analytical methods. For instance, instead of assuming or extrapolating a shape for the viscosity-temperature relation of a given material below the liquidus, this relationship could be derived from analysis of the films. This analysis would proceed as follows:

1. Starting with the temperature-coded films of the crystallization process, the entire experimentally observed growth rate-temperature curve would be generated. By counting frames, for instance, the growth over a small increment of time would be computed. The calculated growth rate would then be referenced to the appropriate mean temperature. This process would then be repeated at successive small time increments during the phase change process. An experimentally observed growth rate-temperature relation would be generated.

2. Assuming an analytical model for the growth process, the viscosity-temperature relation would then be generated. This will enable us to obtain "glassy" data such as viscosity from materials that have never formed glasses. It is believed that the assumption of a particular growth model to give viscosity data in this analysis will give more accurate critical cooling rate data than the converse technique of obtaining the growth behavior from an assumed viscosity model. Choice of which growth model to use might derive from morphological studies of crystallized samples as discussed in Sections 3.3.1.3 and 3.3.2 above.

3. Since growth and nucleation can be considered as independent processes, the remainder of the analysis dealing with heterogeneous nucleation, homogeneous nucleation and critical cooling rates can proceed as in Section 6.1.

The materials for this proposed future work are listed in Table VII. Viscosity data for germania, GeO_2, are readily available since GeO_2 is a well established glass former. No viscosity data exists for the other materials. Therefore, the germania viscosity data extracted from the literature will provide a good check on the accuracy of the above-described analytical-empirical technique to derive viscosity-temperature data below the fusion temperature. In addition, the viscosity-temperature data derived by this technique can be compared to the liquidus temperature viscosity data obtained by using an approximate technique described by Sokolov[44].

7.2 Assessment of Space Processing Candidacy Through Controlled Experiments and Analysis

To predict how a technique such as space processing could be utilized to produce glasses such as mullite that are relatively unobtainable on Earth, a series of controlled laser melting experiments should now be conducted. The emphasis would be in determining the optimum experimental conditions for obtaining near-intrinsic glass formation through in-space processing. Based on our initial work and results described in Section 6.1, it is believed that the mullite system warrants this further work.

The experimental variables for the laser melting experiments that IITRI suggests include: a) the amount of foreign material such as dust particles in the environment, and b) the amount of initial superheating necessary to dissolve surface or internal refractory impurities into the melt without significant sample vaporization. Starting with films of the laser melting experiments conducted under these conditions, IITRI would then perform analyses similar to those conducted on the current program. The result of this work will be a quantitative indication of how close to intrinsic the melting experiments were, and thus a quantitative estimate of the potential of space processing in producing unique glasses unobtainable on earth. IITRI's work on the current program serves as the basis for this prediction method. The Rockwell air suspended laser melting facility provides a unique capability for accomplishing this prediction of the space processing candidacy of mullite, and defining the experimental conditions that must be satisfied for the mission to be successful.

TABLE VII

PROPOSED MATERIALS FOR FUTURE ANALYTICAL AND EMPIRICAL STUDY

Material	Tm(^{o}K)	Entropy of Fusion, Δs_f(cal $mol^{-1}K^{-1}$) [43]
V_2O_5	943	16.5
GeO_2	1389	7.56
Nb_2O_5	1733	16
CoO	2078	5.8
Al_2O_3	2300	11
Y_2O_3	2500	10

8.0 CONCLUSIONS

Prediction of the glass forming tendencies of unique oxide systems will facilitate determination of candidate materials for NASA's Space Processing Program. The ultimate objective of space processing is to produce technically significant glasses by either 1) extending the earth-limited regions of glass formation for certain compositions, or 2) by obtaining glass formation in other compositions that are not glass formers based on empirical earth observations.

IITRI has shown that these goals can be accomplished by modelling the glass forming behavior of selected materials systems through the development of kinetic relationships describing nucleation and crystallization phenomena. The theoretical/analytical background for this has been obtained on IITRI's current program. A fairly comprehensive treatment of nucleation and growth kinetics in pure substances has been presented. The derived transformation kinetics have been successfully applied to a well-characterized system (SiO_2), an excellent glass former (B_2O_3), and a poor glass former by conventional means (Al_2O_3). The kinetic and thermodynamic parameters of viscosity and entropy of fusion were shown to be the primary materials parameters controlling glass forming tendency.

For complex multicomponent systems where diffusional effects predominate, the state-of-the-art is not nearly as far advanced as for simple substances. The transformation kinetics of materials which crystallize with a large compositional change are most probably governed by the long range diffusion of the slowest-moving species. The general lack of specific diffusion data, however, dictate that simplifying assumptions be made, such as the validity of the Stokes-Einstein equation relating bulk diffusion and viscosity.

In addition to diffusion-controlled kinetics, heterogeneous nucleation effects must be considered in real, non-simple systems, since heterogeneous nucleation is the probable cause of the earth-limited glass forming ability in many materials. Where complete

kinetic property data were not available for this analysis, we have shown that the required information can be derived from empirical evidence of the phase change phenomena. This empirical phase transformation information was obtained through a cooperative effort with North American Rockwell Corporation. The Rockwell experiments entailed the air-suspended laser melting of various oxide systems. The nature of the liquid-solid phase transformation (and thus glass forming tendency) was obtained from the analysis of the filmed records of these experiments. Using this analytical/empirical approach the mullite system was analyzed, giving results that 1) are consistent with experimentally observed data, and 2) that indicated the promise of mullite as a future space processing candidate.

This program provides NASA with a means of assessing the candidacy of selected systems for space processing, and determining the experimental-hardware requirements of a successful in-space processing experiment.

Respectfully submitted,
IIT RESEARCH INSTITUTE

D. C. Larsen
Research Engineer
Ceramics Research Section

APPROVED:

S. A. Bortz
Assistant Director
Mechanics of Materials Research Division

REFERENCES

1. Morey, G. W., The Properties of Glass, Reinhold, New York, 2nd Edition (1959).

2. Jackson, K. A., "Nucleation from the Melt," Nucleation Phenomena, American Chemical Society (1966).

3. Turnbull, D., "Thermodynamics and Kinetics of Formation of the Glass State and Initial Devitrification," Physics of Non-Crystalline Solids, Proc. Int'l. Conf., Delft, J. A. Prins., ed. (1964).

4. Hammel, J. J., "Nucleation in Glass Forming Materials," Chapter in Nucleation, A. C. Zettlemoyer, ed., Marcel Dekker, N. Y. (1969).

5. Hillig, W. B., "A Theoretical and Experimental Investigation of Nucleation Leading to Uniform Crystallization of Glass," Symposium on Nucleation and Crystallization in Glasses and Melts, American Ceramic Society (1962).

6. Collins, F. C., Z. Elektrochem. 59 404 (1955).

7. Turnbull, D. and Cohen, M. H., "Crystallization Kinetics and Glass Formation," Modern Aspects of the Vitreous State, Vol. 1, J. D. Mackenzie, ed., Butterworths, London (1960).

8. Uhlmann, D. R. and Chalmers, B., "The Energetics of Nucleation," Nucleation Phenomena, Am. Chem. Soc. (1966).

9. Hammel, J. J., "Nucleation in Glass - A Review," Adv. Nucleation and Crystallization in Glasses, Glass Division Symposium, Am. Ceram. Soc., Sp. Publ. #5, L. L. Hench and S. W. Freiman, eds. (1971).

10. Rawson, H., Inorganic Glass-Forming Systems, Academic Press, New York (1967).

11. Hillig, W. B., "Glass as a Medium for Controlling Physiochemical Reactions," in Reactivity of Solids, J. W. Mitchell, et.al., eds., Wiley (1969).

12. Uhlmann, D. R., "Crystal Growth in Glass-Forming Systems - A Review," Adv. Nucleation and Crystallization in Glasses, Am. Ceram. Soc., Sp. Publ. #5, L. L. Hench and S. W. Freiman, eds. (1971).

13. Uhlmann, D. R., "A Kinetic Treatment of Glass Formation," J. Non-Cryst. Solids 7 337-48 (1972).

REFERENCES (cont'd)

14. Mackenzie, J. D., J. Am. Ceram. Soc. 44(12)(1961) from Parks and Spaght, Physics 6(2)(1935).

15. IITRI Measured Container Composition: $71SiO_2 \cdot 15Na_2O \cdot 8CaO \cdot 4.5MgO \cdot 1.5Al_2O_3$.

16. Reibling, E. F., J. Chem. Phys. 39(7)(1963).

17. "Recommended Values of the Thermophysical Properties of Eight Alloys, Major Constituents and Their Oxides," unpublished compilation of data from Thermophysical Properties Research Center, Purdue University (1966); Source of Data: Kozakevitch, P., Met. Soc. Conf. 7 97 (1961).

18. Fontana, E. H. and Plummer, W. A., "A Study of Viscosity-Temperature Relationships in the GeO_2 and SiO_2 Systems," Phys. Chem. Glasses 7(4)(1966).

19. Bacon. J. F., et. al., "Viscosity and Density of Molten Silica and High Silica Content Glasses," Phys. Chem. Glasses 1 (3) (1960).

20. Brückner, R., "Properties and Structure of Vitreous Silica," J. Non-Cryst. Solids 5(3)(1970).

21. JANAF Thermochemical Data Tables.

22. Brückner, V. R., Glass Tech. Ber. 37(H9) 413 (1964).

23. Macedo, P. B., and Napolitano, A., J. Chem. Phys. 49(4) 1887 (1968).

24. Napolitano, A., Macedo, P. B. and Hawkins, E. G., "Viscosity and Density of Boron Trioxide," J. Am. Ceram. Soc. 48(12) 613 (1965).

25. Turnbull, D. and Cohen, M. H., "Concerning Reconstructive Transformation and Formation of Glass," J. Chem.Phys. 29(5) (1958).

26. Hillig, W. B., private communication.

27. Hammel, J. J., private communication.

28. Frank, F. C., Proc. Roy. Soc. (London) A201 586 (1950).

29. Takamori, T. and Roy, R., "Rapid Crystallization of $SiO_2 \cdot Al_2O_3$ Glasses," J. Am. Ceram. Soc. 56(12) 639-44 (1973).

REFERENCES (cont'd)

30. Happe, R. A., "Manufacturing Unique Glasses in Space", Rockwell International Monthly Progress Report #11 to NASA-MSFC under Contract NAS8-28991 (7 March to 5 April 1974).

31. Touloukian, Y. S., "Recommended Values of the Thermophysical Properties of Eight Alloys, Major Constituents and Their Oxides", unpublished data compilation at the Thermophysical Property Research Center (TPRC, Purdue Univ.); Data Source: Kozakevitch, P. Met. Soc. Conf. 7 97 (1961).

32. Brewer, L., Professor of Materials Science, Univ. of Calif. at Berkeley, private communication.

33. "Selected Values of Critical Thermodynamic Properties", NBS Circular 500.

34. Happe, R. A., "Manufacturing Unique Glasses in Space", Monthly Progress Report No. 6 for the period of 1 October to 31 October 1973. NASA Contract NAS8-28991 (1973).

35. ibid, Monthly Progress Report No. 8 for the period of 1 December to 31 December (1973).

36. Sargeant, P. T., "New Experimental and Theoretical Approaches to the Glassy State", PH.D. Thesis, Solid State Science, Pennsylvania State Univ., (Dec., 1967).

37. Happe, R. A., "Study of the Production of Unique New Glasses", Final Report on Contract NAS8-28014 (estimated from information presented on pages 51-56) (13 June 1972).

38. Rawson, H., Inorganic Glass-Forming Systems, Academic Press, New York (1967).

39. Happe, R. A., "Manufacturing Unique Glasses in Space", NASA-MSFC Contract NAS 8-28991, Sixteenth Monthly Progress Report (17 Sept. 1974).

40. Happe, R. A., "Manufacturing Unique Glasses in Space", NASA-MSFC Contract NAS8-28991, Seventeenth Monthly Progress Report (15 Oct. 1974).

41. Ryshkewitch, E., Oxide Ceramics - Physical Chemistry and Technology, Academic Press, New York (1960).

42. Happe, R. A., Rockwell International, private communication.

43. Handbook of Chemistry and Physics, Chemical Rubber Co., 46th Edition, pages D35-D37 (1964).

44. Sokolov, O. K., "Calculation of Viscosity in Molten Salts (Oxides)", NASA TTF-416 (circa 1962).

BIBLIOGRAPHY

45. Avrami, M., "Kinetics of Phase Change - II: Transformation-Time Relations for Random Distribution of Nuclei." J. Chem. Phys. 8 212 (1940).

46. Berezhonoi, A. I., Glass Ceramics and Photo-Sitalls, Chapter II, "The Formation of Nuclei and the Crystallization of Glass," Mercol, S. A., Pincus, A. G. (trans.) Plenum, New York (1970).

47. Binsbergen, F. L., "Computer Simulation of Nucleation and Crystal Growth," J. Cryst. Growth. 16 249 (1972).

48. Binsbergen, F. L., "Study of Molecular Phenomena in the Nucleation of Crystallization by Computer Simulation and Application to Polymer Crystallization Theory," J. Cryst. Growth 13/14, 44 (1972).

49. Buckle, E. R., "Studies on the Freezing of Pure Liquids, II. The Kinetics of Homogeneous Nucleation in Supercooled Liquids," Proc. Roy. Soc. (London) A261 189 (1961).

50. Calvert, P. D. and Uhlmann, D. R., "Surface Nucleation Growth Theory for the Large and Small Crystal Cases and the Sig ificance of Transient Nucleation," J. Cryst. Growth 12 291 (1972).

51. Cooper, A. R., "Crystal Growth in Network Liquids by Structure Rearrangement," in Adv. Nucleation and Crystallization in Glasses, L. L. Hench and S. W. Frieman, eds., Am. Ceram. Soc. Sp. Publ. #5 (1971).

52. Cooper, A. R. and Gupta, P. K., "Analysis of Diffusion Controlled Crystal Growth in Multicomponent Systems," ibid, pg. 131.

53. Dunning, W. J., "General and Theoretical Introduction (to Nucleation," Chapter in Nucleation, A. C. Zettlemoyer, ed., Marcel Dekker, N. Y. (1969).

54. Eckstein, B., "Vitreous States," Mat. Res. Bull. 3 199-208 (1968).

55. Ewing, R. H., "The Free Energy of the Crystal-Melt Interface from the Radial Distribution Function," J. Cryst. Growth 11 221 (1971).

56. Fisher, J. C., et. al., "Nucleation," J. Appl. Phys. 19 775 (August 1948).

57. Frank, F. C., "An Outline of Nucleation Theory," J. Cryst. Growth 13/14 154 (1972).

58. Ghez, R., "An Exact Calculation of Crystal Growth Rates Under Conditions of Constant Cooling Rate," J. Cryst. Growth 19 153 (1973).

59. Ghez, R. and Lew, J. S., "Interface Kinetics and Crystal Growth Under Conditons of Constant Cooling Rate," J Cryst. Growth 20 273 (1973).

60. Gibbs, J. H., "Nature of the Glass Transition and the Vitreous State," in Modern Aspects of the Vitreous State, I, J. D. Mackenzie, ed.

61. Gilmer, G. H. and Bennema, P., "Computer Simulation of Crystal Surface Structure and Growth Kinetics," J. Cryst. Growth 13/14 148 (1972).

62. Gutzow, I. and Kashchiev, D., "Kinetics of Overall Crystallization of Undercooled Melts in Terms of the Non-Steady State Theory of Nucleation," in Adv. Nuclation and Crystallization in Glasses, L. L. Hench and S. W. Freiman, eds., Am. Ceram. Soc. Sp. Publ. #5 (1971).

63. Hammel, J. J., "Direct Measurements of Homogeneous Nucleation Rates in a Glass-Forming Systems," J. Chem. Phys. 46 (6) 2234 (1966).

64. Heaton, H. M. and Moore, H., "A Study of Glasses Consisting Mainly of the Oxides of Elements of High Atomic Weight, Part III. The Factors Which Determine the Possibility of Glass Formation," J. Soc. Glass Technol. XLI (198) (Feb. 1957).

65. Hillig, W. B., "Kinetics of Solidification from Nonmetallic Liquids," in Kinetics of High Temperature Processes, W. D. Kingery, ed.

66. Hillig, W. B. and Turnbull, D., "Theory of Crystal Growth in Undercooled Pure Liquids," J. Chem. Phys. 24 (4) 914 (1956).

67. Hopper, R. W., et. al., "Crystallization Statistics, Thermal History and Glass Formation," J. Non-Cryst. Solids 15 45-62 (1974).

68. Hopper, R. W. and Uhlmann, D. R., "Solute Redistribution During Crystallization at Constant Velocity and Constant Temperature," J. Cryst. Growth 21 203 (1974).

69. Hopper, R. W. and Uhlmann, D. R., Temperature Distributions During Crystallization at Constant Velocity," J. Cryst. Growth 19 177 (1973).

70. Jackson, K. A., "On Surface Free Energy Calculations," J. Cryst. Growth 10 119 (1971).

71. Jones, D. R. H., "A Mechanical Model of Solid-Liquid Interfaces," J. Cryst. Growth 21 167 (1974).

72. Knight, C. A., "Breeding of Crystal Nuclei by Classical Nucleation: Theory and Some Observations and Experiments," J. Cryst. Growth 11 201 (1971).

73. Konak, A. R., "Difficulties Associated with Theories of Growth from Solution," J. Cryst. Growth 19 247 (1973).

74. Lothe, J. and Pound, G. M., "Statistical Mechanics of Nucleation," Chapter in Nucleation, A. C. Zettlemoyer, ed., Marcel Dekker, N. Y. (1969).

75. MacDowell, J. F., "Nucleation in Glasses," in Nucleation Phenomena, Am. Chem. Soc. (1966).

76. Magill, J. H. and Li, H. M., "A Corresponding States Equation for Crystallization Kinetics," J. Cryst. Growth 19 361 (1973).

77. Markov, I. and Kashchiev, D., "Nucleation on Active Centres 1. General Theory," J. Cryst. Growth 16 170 (1972).

78. McMillan, P. W., Glass-Ceramics, Chapter 2, "Crystallization and Devitrification," Academic Press, N. Y. (1964).

79. Robertson, D. and Pound, G. M., "Numerical Simulation of Heterogeneous Nucleation and Growth, J. Cryst. Growth 19 269 (1973).

80. Sargeant, P. and Roy, R., "New Approach to the Prediction of Glass Formation," Mat. Res. Bull. 3 265-80 (1968).

81. Sears, G. W., "Recent Developments in Nucleation Theory," in Physics and Chemistry of Ceramics, C. Klingsberg, ed., Gordon and Breach (1963).

82. Stevels, J. M., "Permitted and Forbidden Structural Units in Vitreous Systems," Mat. Res. Bull. 3 599-610 (1968).

83. Sun, K., "Fundamental Condition of Glass Formation," J. Am. Ceram. Soc. 30 (9) 277 (1947).

BIBLIOGRAPHY (Cont'd.)

84. Tashiro, M., "Nucleation and Crystal Growth in Glasses," Eighth International Congress on Glass (1968).

85. Turnbull, D., "Phase Changes," in Solid State Physics - Advances in Research and Applications, Vol. 3, Academic Press, N. Y. (1956).

86. Turnbull, D., "Under What Conditions Can a Glass be Formed?" Contemp. Phys. 10 (5) 473-88 (1969).

87. Turnbull, D. and Cohen, M. H., "Free-Volume Model of the Amorphous Phase: Glass Transition," J. Chem. Phys. 34 (1) 120 (1961).

88. Walton, A. G., "Nucleation in Liquids and Solutions," Chapter in Nucleation, A. C. Zettlemoyer, ed., Marcel Dekker, N. Y. (1969).

89. Walton, A. G., "Bulk and Surface Transport in Liquids - An Introudctory Treatment," Contemp. Phys. 10 (5) 489 (1969).

90. White, W. B. and Berkes, J. S., "Calculation of Volume Free Energy of Nucleation of a Crystalline Phase from a Multi-component Regular Solution," J. Am. Ceram. Soc. 52 (4) 231 (1969).